

1  
2  
3  
4  
5  
6  
7  
8  
9  
10  
11  
12  
13  
14

**Identification of a bile acid-binding transcription factor in *Clostridioides difficile* using chemical proteomics**

Forster ER<sup>1,2</sup>, Yang X<sup>3</sup>, Hang HC<sup>3,4</sup>, Shen A<sup>2</sup>

<sup>1</sup>Graduate School of Biomedical Sciences, Tufts University, Boston MA, USA

<sup>2</sup>Department of Molecular Biology and Microbiology, Tufts University School of Medicine, Boston MA, USA

<sup>3</sup>Department of Immunology and Microbiology, Scripps Research, La Jolla CA, USA

<sup>4</sup>Department of Chemistry, Scripps Research, La Jolla CA, USA

15 **Abstract**

16

17 *Clostridioides difficile* is a Gram-positive anaerobic bacterium that is the leading cause of hospital-  
18 acquired gastroenteritis in the US. In the gut milieu, *C. difficile* encounters microbiota-derived bile  
19 acids capable of inhibiting its growth, which are thought to be a mechanism of colonization  
20 resistance. While the levels of certain bile acids in the gut correlate with susceptibility to *C. difficile*  
21 infection, their molecular targets in *C. difficile* remain unknown. In this study, we sought to use  
22 chemical proteomics to identify bile acid-interacting proteins in *C. difficile*. Using photoaffinity bile  
23 acid probes and chemical proteomics, we identified a previously uncharacterized MerR family  
24 protein, CD3583 (now BapR), as a putative bile acid-sensing transcription regulator. Our data  
25 indicate that BapR binds and is stabilized by lithocholic acid (LCA) in *C. difficile*. Although loss of  
26 BapR did not affect *C. difficile*'s sensitivity to LCA,  $\Delta bapR$  cells elongated more in the presence  
27 of LCA compared to wild-type cells. Transcriptomics revealed that BapR regulates the expression  
28 of the gene clusters *mdeA-cd3573* and *cd0618-cd0616*, and *cwpV*, with the expression of the  
29 *mdeA-cd3573* locus being specifically de-repressed in the presence of LCA in a BapR-dependent  
30 manner. Electrophoretic mobility shift assays revealed that BapR directly binds to the *mdeA*  
31 promoter region. Since *mdeA* is involved in amino acid-related sulfur metabolism and the *mdeA-*  
32 *cd3573* locus encodes putative transporters, we propose that BapR senses a gastrointestinal  
33 tract-specific small molecule, LCA, as an environmental cue for metabolic adaptation.

34

35

## 36 Introduction

37

38 *Clostridioides difficile* is a Gram-positive, anaerobic, spore-forming bacterium that is a  
39 leading cause of nosocomial gastroenteritis worldwide (1, 2). In 2017, *C. difficile* was responsible  
40 for ~460,000 infections and ~13,000 deaths in the United States alone (3). *C. difficile* infections  
41 (CDIs) are transmitted by its aerotolerant spores, which germinate in the distal small intestine in  
42 response to cholate-derived bile acids, giving rise to toxin-producing vegetative cells that colonize  
43 the colon (4). While prior antibiotic use and the consequent disruption of the gut microbiota is a  
44 primary risk factor for CDI, the specific mechanisms by which the microbiota protect against CDI  
45 remain largely unknown. However, production of secondary bile acids by the gut microbiota has  
46 been proposed to be a major contributor to colonization resistance. Bacteria that produce  
47 secondary bile acids are sufficient to confer colonization resistance against CDI, and the levels of  
48 these secondary bile acids in the gut correlate with resistance to CDI (4–8). Additionally, *C. difficile*  
49 is highly sensitive to growth inhibition by secondary bile acids, with lithocholic acid (LCA) and its  
50 derivatives being the most potent inhibitors (6, 7, 9).

51 Bile acids are amphipathic, detergent-like molecules produced by the liver and secreted  
52 into the small intestine to aid in fat digestion. Host-derived primary bile acids are largely  
53 reabsorbed via enterohepatic recirculation in the distal small intestine, but approximately 5%  
54 reach the large intestine where they are transformed into secondary bile acids by the microbiota  
55 (10). In cecal samples obtained from individuals who died an unnatural death, total bile acids were  
56 measured at ~200 - 1,000  $\mu\text{M}$  (11). This pool consisted mostly of the secondary bile acids LCA  
57 and deoxycholic acid (DCA): on average, each represented ~25-33% of the bile acids in the non-  
58 CDI cecum (11) and feces (10). Growing evidence suggests that microbiota-derived secondary  
59 bile acids have broad pathophysiological implications in the host from carcinogenesis (12) to  
60 immune modulation and inflammation (13–20) to pathogen resistance (9, 21, 22), including *C.*

61 *difficile*. Indeed, bile acids cause a broad range of stresses in bacteria including membrane  
62 disruption, protein denaturation, iron and calcium chelation, and DNA damage (23, 24).

63 DCA and LCA are made from the primary bile acids cholic acid (CA) and chenodeoxycholic  
64 acid (CDCA), respectively, via 7 $\alpha$ -dehydroxylation by a select few members of the gut microbiota  
65 (25–31). This activity is encoded by the bile acid-inducible (*bai*) operon (25–31), which is highly  
66 correlated with resistance to CDI in animal models (7, 30, 31). A few *bai* operon-positive  
67 *Clostridium* species, namely *C. scindens*, are each sufficient to protect mice against CDI (7, 32,  
68 33), although *bai* operon mutant strains have not yet been tested presumably due to genetic  
69 limitations. Notably, sequestration of bile from the cecal contents of *C. scindens*-colonized mice  
70 with cholestyramine is sufficient to rescue *C. difficile* growth *ex vivo*, suggesting that the bile acids  
71 produced by *C. scindens* inhibit *C. difficile* infection (7). Further, DCA and LCA are undetectable  
72 in the cecal contents of antibiotic-treated mice and recurrent CDI patient feces, but they are  
73 present in gut environments that are inhibitory to *C. difficile* (4–6, 8, 34). Underscoring these  
74 correlations, concentrations of DCA and LCA present in CDI-resistant mice are sufficient to inhibit  
75 *C. difficile* growth *in vitro* (6), and LCA tolerance correlates with virulence across *C. difficile* strains  
76 in a murine model of infection (35). While subsequent studies suggest that 7 $\alpha$ -dehydroxylating  
77 bacteria also inhibit *C. difficile* through bile acid-independent mechanisms such as antibiotic  
78 production and competition for Stickland metabolism substrates (32, 36), secondary bile acids  
79 nonetheless appear to be a major contributor.

80 Gut commensals and several gut pathogens have evolved mechanisms to resist or  
81 tolerate the toxicity of bile acids (23, 24, 37), yet resistance mechanisms remain undefined in *C.*  
82 *difficile*. Currently, little is known about *C. difficile*'s interactions with bile acids at the molecular  
83 level, although bile acids have been shown to modulate several aspects of *C. difficile* physiology.  
84 LCA causes loss of flagella and cell elongation (38) whereas DCA induces biofilm formation and  
85 represses sporulation (39). Toxin expression and/or activity is inhibited by LCA, DCA,  
86 isolithocholic acid (isoLCA), isodeoxycholic acid, and ursodeoxycholic acid, and the TcdB toxin

87 was recently shown to bind several bile acids (39–41). This latter observation represents the sole  
88 biochemical evidence of a *C. difficile* protein specifically binding to a bile acid to date. Indeed,  
89 while genetic studies suggest that the CspC pseudoprotease is a receptor for the primary bile  
90 acid germinant, taurocholic acid (TCA) (42), direct binding of TCA or other cholate-derived bile  
91 acid germinants (43) to *C. difficile* spore proteins has not been demonstrated. Furthermore, no  
92 targets of bile acids in *C. difficile* vegetative cells have been identified.

93 In this study, we employed recently developed photoaffinity bile acid probes in a chemical  
94 proteomics screen to identify the targets of toxic bile acids in vegetative *C. difficile*. While our  
95 screen identified several essential proteins as targets of LCA-derived probes, a putative MerR  
96 family transcription factor, CD3583 (now BapR), was highly enriched. Here, we demonstrate that  
97 BapR binds to LCA in *C. difficile*. BapR appears to modulate cell length in response to LCA and  
98 directly represses the expression of a locus encoding genes involved in sulfur metabolism. Our  
99 data also indicate that BapR indirectly represses the expression of two additional loci encoding  
100 two other putative transcription factors and the cell wall protein CwpV.

101

## 102 **Results**

103

### 104 **Bile acid probes label distinct *C. difficile* proteins in a dose-dependent manner**

105

106 Coupling photoaffinity probes of microbiota metabolites with chemical proteomics affords  
107 new opportunities to characterize specific protein targets and elucidate small molecule  
108 mechanisms of action (44). For example, bile acid photoaffinity probes recently identified the HilD  
109 regulator of SPI-1 virulence gene expression as a target of CDCA in *Salmonella* Typhimurium  
110 (Yang X, Stein K, Hang HC in revision). Using a similar approach, we sought to uncover the  
111 targets of bile acids in *C. difficile* to gain insight into the mechanism of inhibition by DCA or LCA  
112 and potential

113 adaptation of *C. difficile* to these toxic, microbiota-derived molecules. These probes are generated  
114 from naturally occurring bile acids with the addition of two functional groups for photocrosslinking  
115 and bioorthogonal detection (**Figure 1A**). The diazirine functional group allows for covalent  
116 crosslinking to interacting proteins using UV light, while the terminal alkyne tag allows for  
117 detection or isolation of interacting proteins after bioorthogonal labeling with fluorophore-azide or  
118 biotin-azide reagents, respectively (**Figure 1B**).

119 To gain insight into how toxic bile acids affect *C. difficile*'s physiology, we sought to identify  
120 targets of these microbiota-derived molecules. Since LCA potently inhibits growth of *C. difficile*,  
121 we employed LCA-derived probes to identify LCA's cellular targets. Using growth inhibition in  
122 broth culture as a readout of probe activity, we found that Probe 8 potently inhibited growth with  
123 an IC<sub>50</sub> of ~10 μM (**Figure 1C**). This inhibition was comparable to the IC<sub>50</sub> of isoallothiocholic acid  
124 (isoalloLCA, ~2 μM, **Figure 1D**), which was recently identified as an especially toxic bile acid to  
125 *C. difficile* in the gut of centenarians (9). Although solubility limited the range of concentrations we  
126 could test, Probe 8 was more potent than LCA (IC<sub>50</sub> ~50 μM) and DCA and CDCA (IC<sub>50</sub>s of ~100  
127 μM, **Figure 1D and Figure S2**). The primary bile acids CA and TCA did not inhibit growth up to  
128 400 μM (**Figure 1D and Figure S2**). Importantly, we observed these effects at physiologically  
129 relevant concentrations since LCA and DCA have been measured at 1 - 450 μM and 30 - 700 μM,  
130 respectively, in non-CDI human cecal contents (11) and ~1 mM and ~1.2 mM, respectively, in  
131 human feces post-FMT (34). Interestingly, Probe 3 did not appreciably inhibit the growth of *C.*  
132 *difficile* (**Figure 1C**) despite sharing LCA as a parent structure with Probe 8. Due to its structural  
133 similarity to Probe 8 yet substantially reduced growth inhibitory activity, we selected Probe 3 as a  
134 control probe.

135 To qualitatively assess whether the probes specifically interact with proteins in *C. difficile*,  
136 we used fluorescent SDS-PAGE to visualize labeling. To this end, we treated log-phase *C. difficile*  
137 cultures with 2.5 or 25 μM Probe 8 or DMSO vehicle for 30 minutes, washed cells to remove  
138 unbound probe, and UV irradiated cells to covalently link the probe to interacting proteins. After

139 generating total cell lysate and performing a click reaction in the total lysate to conjugate  
140 AlexaFluor-488-azide to the probe, these probe-bound proteins were visualized by SDS-PAGE  
141 using fluorescent imaging (**Figure 1B**). We observed distinct bands in a dose- and UV-dependent  
142 manner indicative of Probe 8 interacting with specific *C. difficile* proteins (**Figure 1E**). Possibly in  
143 line with its reduced growth inhibitory activity, Probe 3 exhibited weaker labeling (**Figure S1**).

144

### 145 **Chemical proteomics identifies bile acid-binding proteins in *C. difficile***

146

147 To identify the direct targets of Probe 8 visualized in the in-gel fluorescence assay, we  
148 used a chemical proteomics approach to enrich for probe-bound proteins. After conjugating biotin-  
149 azide onto probe-bound proteins (**Figure 1B**), we used streptavidin beads to isolate the proteins  
150 that interacted with Probe 8 and/or Probe 3 after 1 hour of treatment during log-phase (**Figure**  
151 **S1**). Streptavidin-enriched proteins were then identified using label-free quantitative liquid  
152 chromatography-tandem mass spectrometry (**Figure 1F and Table S1**). These proteomic  
153 analyses revealed 48 hits for Probe 8 and 52 hits for Probe 3 relative to DMSO (modified Z score >  
154 3). Of the Probe 8 hits, 27 were specific to Probe 8 over Probe 3 (**Figure 1G**). We were particularly  
155 interested in Probe 8-specific proteins because Probe 8 is associated with growth inhibitory  
156 activity. Consistent with the toxicity of Probe 8 and its parent LCA molecule, 9 of the 27 hits  
157 specific to Probe 8 were essential (45). These included proteins involved in DNA replication,  
158 transcription, or cell division, namely DnaA, NusA, and MinD. The coenzyme A synthesis protein  
159 CoaBC and fatty acid synthesis protein FabD were additional essential hits. The essential cell  
160 wall synthesis protein MurC was of particular interest considering that *C. difficile* cells elongate  
161 with LCA treatment (38). However, the most enriched protein from our screen was a non-essential  
162 MerR family transcription factor, CD3583 (herein bile acid-binding protein regulator BapR; locus  
163 tag CD630\_35830) (**Figure 1F**). MerR family transcription factors typically regulate efflux pumps  
164 that export the toxic molecules they sense (46) and can function as repressors in the absence of

165 ligand as well as activators upon ligand binding. Given the role of MerR family transcription factors  
166 in regulating resistance or adaptative responses, we sought to explore the function of BapR in *C.*  
167 *difficile*.

168

### 169 **BapR specifically binds LCA-derived bile acids**

170

171 Structural modeling using iTASSER (47) predicted that BapR is highly similar to a MerR  
172 family transcription factor in *Bacillus subtilis*, BmrR. BapR shares 18% identity and 28% similarity  
173 with BmrR, most of which is in the N-terminal region. MerR family transcription factors have  
174 conserved N-terminal DNA binding domains and variable C-terminal ligand-binding domains.  
175 These ligand binding domains have been observed to sense and respond to a wide diversity of  
176 molecules, with ligands ranging from metal ions to large amphipathic drugs (48). Although BmrR  
177 does not bind bile acids, its ligands are large hydrophobic molecules with some similarity to the  
178 sterol center of bile acids (49–51).

179 To validate BapR as a target of Probe 8, we used an independent method for assessing  
180 whether the bile acid probes could pull down BapR from *C. difficile*. Specifically, we treated *C.*  
181 *difficile* cultures expressing a FLAG-tagged allele of *bapR* from its native locus with either DMSO,  
182 Probe 8, or Probe 3 for 1 hour during log-phase. The probe was UV crosslinked to its protein  
183 targets, and then the cells were lysed. After conjugating biotin-azide to probe-bound proteins  
184 using click chemistry, we isolated these proteins using streptavidin beads (**Figure 1B**). FLAG-  
185 tagged BapR was enriched in the pull-downs using Probe 8, and to a lesser extent using Probe  
186 3, relative to DMSO-treated cultures (**Figure 2A**, representative of three biological replicates).  
187 More biotinylated probe-bound protein was present in the Probe 8 pull-downs relative to Probe 3  
188 as detected with fluorescent streptavidin, consistent with Probe 8 interacting with more proteins  
189 in our proteomics screen (**Figure 1F and Table S1**).



190 To determine whether we could directly detect binding between BapR and LCA, we used  
191 thermal shift assays to compare the relative affinity of BapR for different bile acids. Thermal shift  
192 assays (also known as differential scanning fluorimetry, DSF) measure the change in melting  
193 temperature ( $T_m$ ) of a protein in the presence of a ligand using a fluorescent dye that binds to  
194 hydrophobic regions of a protein as it unfolds. While ligand binding typically increases the  $T_m$  of a  
195 protein because ligand binding stabilizes proteins, it can in some instances decrease the  $T_m$  if the  
196 conformation stabilized by the ligand melts more readily (52). An example of this phenomenon  
197 can be found in isoLCA binding to the eukaryotic AKR1A1 aldo-keto reductase, for which isoLCA  
198 is a known ligand (53). Like AKR1A1, we observed a dose-dependent decrease in  $T_m$  when  
199 purified BapR (**Figure 2C**) was incubated with increasing concentrations of Probe 8 and certain  
200 bile acids in the presence of SYPRO Orange dye (**Figure 2D and E**). Specifically, we detected a  
201  $\sim 4^\circ\text{C}$   $T_m$  shift with 32  $\mu\text{M}$  Probe 8 compared to a  $\sim 1^\circ\text{C}$   $T_m$  shift with Probe 3 at the same  
202 concentration. We also observed up to a  $\sim 5^\circ\text{C}$   $T_m$  shift at 64  $\mu\text{M}$  LCA, whereas DCA and CDCA  
203 required  $\sim 10$ -fold higher concentrations (500  $\mu\text{M}$ ) to shift the  $T_m$  of BapR by  $\sim 3^\circ\text{C}$ . Furthermore,  
204 CA and TCA were only able to shift the  $T_m$  by  $\sim 1$ - $2^\circ\text{C}$  at 2 mM. It should be noted that the maximum  
205 concentration shown for each ligand tested was limited by measuring the non-specific interactions  
206 of a given bile acid with the SYPRO Orange dye (i.e. in the absence of BapR).

207 The apparent affinity of BapR for specific bile acids (LCA > DCA/CDCA > CA/TCA)  
208 correlates with fewer hydroxyl groups on the  $\alpha$  face of the steroid center (**Figure 2B**), suggesting  
209 that hydrophobicity of the bile acid influences its interaction with BapR. IsoalloLCA differs from LCA  
210 in the orientation of the 3-OH and most notably by the stereochemistry at carbon 5: the  $5\beta$   
211 hydrogen in LCA results in a “bent” steroid ring, whereas the  $5\alpha$  hydrogen in isoalloLCA results  
212 in a more planar conformation. Interestingly, BapR appeared to have higher affinity for isoalloLCA  
213 given that it induced a  $\sim 5^\circ\text{C}$   $T_m$  shift at a 2-fold lower concentration than LCA (32  $\mu\text{M}$  vs. 64  $\mu\text{M}$ ,  
214 **Figure 2E**). The hydroxyl at carbon 3 is on the  $\beta$  face of the steroid center of isoalloLCA opposed

215 to the  $\alpha$  face for LCA, further implying that hydrophobicity of the  $\alpha$  face is important for interaction  
216 with BapR.

217

### 218 **BapR influences cell length and interacts with LCA in *C. difficile***

219

220 After confirming that BapR binds bile acids, we sought to determine the physiological  
221 function of BapR in *C. difficile*. We initially hypothesized that BapR regulates resistance to bile  
222 acids like other MerR family transcription factors that regulate resistance to their ligands (48).  
223 However, we were unable to detect a growth defect for *C. difficile* lacking *bapR* in the presence  
224 of LCA (**Figure 3A**) or isoalloLCA (**Figure S3**). Besides growth inhibition, cell elongation and loss  
225 of flagella are the only known effects of LCA on *C. difficile* (38), so we instead asked whether  
226 BapR influences these phenotypes. While BapR did not influence motility on soft agar (data not  
227 shown), we observed that loss of BapR resulted in cells elongating ~25% more than wild-type  
228 (WT) cells after a 3-hour exposure to 20  $\mu$ M LCA (**Figure 3B**). Specifically, although LCA  
229 treatment increased the length of WT *C. difficile* cells by ~2  $\mu$ m,  $\Delta$ *bapR* cells elongated an  
230 additional ~0.5  $\mu$ m over the WT strain under these conditions (**Figure 3C**). This phenotype was  
231 complemented by expressing *bapR* from its native promoter at the ectopic *pyrE* locus on the  
232 chromosome ( $\Delta$ *bapR/bapR*; **Figure 3C**) (54). We did not observe gross morphological differences  
233 aside from cell length between the strains upon LCA exposure.

234 To gain initial mechanistic insight into BapR's response to bile acids in *C. difficile*, we  
235 asked whether *bapR* expression changes during bile acid-mediated stress. To this end, we  
236 measured *bapR* transcript levels by qRT-PCR after 1-hour exposure to 20  $\mu$ M LCA or DMSO  
237 vehicle during log-phase. Expression of *bapR* decreased ~3-fold in the WT strain upon LCA  
238 treatment (*bapR* transcript was undetectable in the  $\Delta$ *bapR* strain as expected) (**Figure 4A**).  
239 Despite the unanticipated overexpression of *bapR* in the  $\Delta$ *bapR/bapR* complement strain, *bapR*  
240 expression was down-regulated upon treatment of these cells with LCA (**Figure 4A**).

241           Since our finding that *bapR* expression decreased in response to LCA was somewhat  
242 surprising, we wondered whether this decrease corresponded to lower protein levels. To test this  
243 possibility, we treated log-phase *C. difficile* cultures with increasing concentrations of LCA, DCA,  
244 CDCA, TCA, or isoalloLCA for 3 hours during log-phase and assessed BapR levels by Western  
245 blot. Unexpectedly, we observed a dose-dependent increase in BapR levels with LCA, and to a  
246 lesser extent with DCA, CDCA, and isoalloLCA (**Figure 4B and C**). This implies that BapR is  
247 stabilized by these bile acids or becomes less susceptible to degradation in *C. difficile*, since *bapR*  
248 transcript levels are decreased upon LCA treatment (**Figure 4A**). The elevated BapR levels were  
249 sustained for at least 6 hours of growth with LCA (**Figure S4**). In agreement with the apparent  
250 binding affinity measured in thermal shift assays, ~10-fold higher concentrations of DCA and  
251 CDCA were needed to stabilize BapR at levels comparable to LCA (~3-fold increase at 50  $\mu$ M  
252 LCA vs. ~2-fold increase at 500  $\mu$ M DCA or CDCA). TCA did not change BapR levels even at 500  
253  $\mu$ M, and since BapR did not appreciably bind TCA in our thermal shift assays, the elevated BapR  
254 levels in *C. difficile* seen upon treatment with the other bile acids is likely due to binding. It is  
255 unclear why isoalloLCA increased BapR levels less than LCA in WT *C. difficile* and more in the  
256 complementation strain, but these data nevertheless suggest that BapR interacts with bile acids  
257 in *C. difficile*.

258

### 259 **BapR controls gene expression, in some cases in an LCA-dependent manner**

260

261           Since BapR is predicted to be a MerR-type transcription factor, we next asked whether it  
262 regulates gene expression, particularly in an LCA-dependent manner. To this end, we assessed  
263 the transcriptome of WT and  $\Delta$ *bapR* *C. difficile* during short-term LCA exposure using RNA-seq.  
264 Log-phase cultures of each strain were treated with 20  $\mu$ M LCA or DMSO vehicle for 1 hour before  
265 harvesting RNA for next-generation sequencing. Transcriptomic analysis revealed that LCA  
266 induced global changes in gene expression (569 genes significantly upregulated and 580 genes

267 significantly downregulated;  $p < 0.05$  and fold change  $> 2$ ) (**Figure S5A** and **Table S2**). We noted  
268 changes in line with previously reported effects of LCA on *C. difficile*: motility genes were largely  
269 downregulated in our analyses, consistent with LCA causing loss of flagella (38) (**Figure S5B**).  
270 While the expression of many genes was altered by LCA, we were most interested in genes  
271 whose expression was modulated in a BapR-dependent manner. We found that BapR  
272 significantly influenced the expression of three gene loci: *mdeA-cd3576* (CD630\_35770-  
273 CD630\_35760), *cd0618-cd0616* (CD630\_06180-CD630\_06160), and *cwpV* (CD630\_05140)  
274 (**Figure 5A**). Expression of these genes was higher in the  $\Delta bapR$  strain relative to WT (2-4-fold  
275 different), indicating that BapR represses them.

276         Of the genes significantly affected by BapR, *mdeA* and *cd3576* expression changed the  
277 most between DMSO and LCA conditions. These genes were differentially expressed in the  
278 DMSO control (WT vs.  $\Delta bapR$ ) but not in the presence of LCA (**Figure 5A**). *mdeA* encodes a  
279 methionine  $\gamma$ -lyase thought to be responsible for methanethiol and  $H_2S$  production from  
280 methionine and homocysteine/cysteine, respectively, (55). *cd3576* encodes a major facilitator  
281 superfamily (MFS) transporter. These genes are found in close proximity to the upstream genes,  
282 *cd3575-cd3573* (**Figure 5B**), which are predicted to encode two hypothetical proteins and a  
283 sodium:solute symporter, respectively. While genome-wide transcription start site (TSS) mapping  
284 in *C. difficile* predicts promoters at *cd3578* and *cd3571*, no TSSs were reported for *mdeA-cd3572*  
285 (56) (**Figure 5B**), although in our experience these genome-wide analyses do not capture all TSS.  
286 Since *cd3573-cd3575* approached significance under at least one condition (*cd3572* and *cd3578*  
287 did not) and may be co-transcribed with *cd3576* and *mdeA* based on proximity and orientation,  
288 we validated expression of *mdeA-cd3573* using qRT-PCR. In line with our RNA-seq analyses, we  
289 found that all genes in this cluster were expressed more in the  $\Delta bapR$  strain than WT under both  
290 conditions, and the differential expression was complemented in the  $\Delta bapR/bapR$  strain (**Figure**  
291 **5C**). Additionally, LCA increased the expression of all genes in the cluster across all strains  
292 (**Figure 5C**). To compare the response to LCA between strains, we plotted expression levels for

293 a given strain as the fold-change in LCA relative to DMSO (LCA/DMSO). This revealed that the  
294 loss of BapR resulted in a smaller induction of these genes in the presence of LCA relative to WT  
295 levels (**Figure 5D**); the differential response was most apparent for *mdeA* and *cd3576* (~6-fold  
296 induction in the WT and complement strains vs. ~1.5-fold induction in the  $\Delta bapR$  strain). Taken  
297 together these data suggest that BapR is necessary to induce these genes in response to LCA,  
298 likely by de-repressing their expression upon sensing LCA.

299 In contrast, *cwpV*, which was differentially expressed between  $\Delta bapR$  and WT *C. difficile*  
300 in our RNA-seq analyses, was not affected by LCA treatment (**Figure 5A**). CwpV is a cell wall  
301 protein that makes up ~13% of the total surface layer proteins in *C. difficile* (57). It promotes  
302 aggregation of *C. difficile* cells *in vitro* (57) and confers resistance to *Siphoviridae* and *Myoviridae*  
303 family phages (58), but is expressed by only ~5% of cells in culture due to a phase-variable RecV-  
304 controlled genetic switch located between its promoter and coding DNA sequence (59). In bulk  
305 population measurements by qRT-PCR, *cwpV* expression was higher in the  $\Delta bapR$  strain than  
306 WT and the complement, particularly in the presence of LCA (**Figure 5E**). However, the fold-  
307 change in *cwpV* expression induced by LCA (~2.5-fold in WT) was the same for  $\Delta bapR$  and the  
308  $\Delta bapR/bapR$  complementation strain (**Figure 5F**). These data suggest that BapR indirectly  
309 represses *cwpV*, since the LCA-induced upregulation of *cwpV* is not dependent on BapR. Given  
310 that LCA causes global changes in the *C. difficile* transcriptional landscape (**Figure S5**), other  
311 unknown factors likely mediate the LCA-induced expression of *cwpV*.

312 Our RNA-seq analyses also identified a second cluster of genes whose expression  
313 changed in a BapR-dependent manner: *cd0618-0616*. The differential expression of *cd0616* and  
314 *cd0617* hovered at the significance cutoff, and *cd0618* approached significance under both  
315 conditions (**Figure 5A**). *cd0618* encodes a LytTR family transcription factor; *cd0617* encodes a  
316 CPBP family intramembrane metalloprotease; and *cd0616* encodes another MerR family  
317 transcription factor. TSSs were previously predicted for *cd0616* and *cd0618*, but not for *cd0617*  
318 (56) (**Figure 5B**). qRT-PCR analyses confirmed that these genes are over-expressed in the

319  $\Delta bapR$  strain relative to WT and the complement strain (**Figure 5G**), but only the expression of  
320 *cd0616* and *cd0617* was affected by LCA treatment (~2-fold reduction) (**Figure 5H**). LCA had  
321 similar effects on the expression of these genes between strains irrespective of whether BapR  
322 was present, indicating that like *cwpV*, BapR does not control their LCA-dependent expression  
323 (**Figure 5H**). While it is unclear whether there are other conditions in which BapR derepresses  
324 the expression of *cwpV* or the *cd0618-cd0616* locus, our data nonetheless imply that (i) BapR  
325 represses gene expression directly and indirectly and that (ii) separate, unknown mechanisms of  
326 LCA-dependent transcriptional regulation act in parallel to BapR.

327

### 328 **BapR binds the promoter region of *mdeA* but not *cd0616***

329

330 To test whether BapR directly regulates the *mdeA* cluster, *cd0618* cluster, or *cwpV*, we  
331 performed electrophoretic mobility shift assays (EMSAs) with the promoter regions of these genes.  
332 These DNA fragments were fluorescently labeled at their 5' ends and incubated with purified  
333 BapR. Dose-dependent mobility shifts of the *mdeA* promoter region were observed for BapR, and  
334 importantly, this shift was competed away by an excess of the same promoter region lacking the  
335 fluorescent label (cold competitor; **Figure 6A**). In line with our transcriptional analyses suggesting  
336 that BapR indirectly regulates *cwpV*, no shift was seen for the *cwpV* promoter in its "on" orientation  
337 (**Figure 6B**) Further, BapR did not bind the promoters of *cd0618* or *cd0616* (**Figure S6**). BapR  
338 failed to bind its own promoter region indicating that it does not autoregulate (**Figure S6**).

339 Notably, we found that LCA addition to the EMSAs did not affect BapR binding to the  
340 *mdeA* promoter (**Figure 6A**). This result was not necessarily surprising given that MerR family  
341 transcription factors remain bound to their DNA targets regardless of whether their C-terminal  
342 domain has bound their ligands. Instead, ligand binding results in these transcription factors  
343 regulating transcription via DNA distortion to reorient the -35 and -10 sites and facilitate productive  
344 RNA polymerase interactions (51, 60, 61). Since MerR family proteins can act as repressors in

345 the absence of ligand and activators in the presence of ligand, our finding that BapR binds the  
346 *mdeA* promoter independently of LCA (**Figure 6A**) is consistent with previously characterized  
347 members of this family (60, 62–64). Furthermore, since BapR maintains the ability to bind DNA  
348 even in the presence of a large molar excess of LCA (**Figure 6A**), the reduced thermal stability  
349 of BapR observed in the presence of LCA (**Figure 2D**) is consistent with BapR undergoing a  
350 conformational change, rather than being destabilized by LCA.

351

## 352 **Discussion**

353

354 In this study, we identified BapR as a novel sensor for bile acids in *C. difficile* that de-  
355 represses the expression of a small subset of genes upon sensing LCA-related bile acids. Our  
356 chemical proteomics, affinity pull-downs, and thermal shift assays indicate that BapR specifically  
357 binds bile acids, especially LCA (**Figure 2**). Our data further suggest that BapR is stabilized by  
358 bile acids in *C. difficile* (**Figure 4**), which allows in BapR to directly de-repress the expression of  
359 genes encoding the methionine  $\gamma$ -lysase MdeA and two putative transporters. Specifically, our  
360 data indicate that BapR binds the promoter region of *mdeA* and represses the expression of the  
361 *mdeA* gene cluster in the absence of LCA; however, upon binding LCA, BapR undergoes a  
362 conformational change that reorients the *mdeA* promoter and licenses transcription (**Figure 7**).  
363 Given MdeA's involvement in sulfur metabolism (55) and the fact that bile acids are found  
364 exclusively in the gut of metazoans, we hypothesize that this LCA-sensing system regulates *C.*  
365 *difficile*'s metabolic adaptation to the gut environment. Since cysteine is elevated ~6-fold in the  
366 dysbiotic murine cecum (5), it is plausible that *C. difficile* would upregulate cysteine catabolism in  
367 this environment. Other factors downstream of this metabolic adaptation may be responsible for  
368 the cell length phenotype (**Figure 3**), but further studies are needed to delineate connections  
369 between these observations. Our RNA-Seq and qRT-PCR analyses also revealed that the  
370 expression of genes encoding the cell surface protein, CwpV, two other transcription factors, and

371 a putative metalloprotease is repressed by BapR (**Figures 5 and 6**), but conditions under which  
372 BapR may de-repress these genes remain to be determined.

373         Although BapR does not appear to be involved in resistance to LCA in the broth culture-  
374 based growth conditions tested, it is possible that the fitness of the  $\Delta bapR$  strain would be reduced  
375 in competition with WT *in vitro* or *in vivo*. It is also possible that *C. difficile* has factors redundant  
376 to BapR that compensate for its loss. However, the strong correlation between presence of DCA  
377 and LCA in the gut and resistance to CDI could indicate that *C. difficile* does not have effective  
378 resistance mechanisms for these microbiota-generated metabolites. Instead, *C. difficile* appears  
379 to grow opportunistically in gut environments with very low levels of DCA and LCA (4–7), where  
380 these low levels could serve as environmental cues. Another possibility is that other stressors in  
381 the gut milieu could potentiate LCA's toxicity and reveal a resistance role for BapR. For example,  
382 antibiotics produced by 7 $\alpha$ -dehydroxylating bacteria like *C. scindens*, which secretes 1-acetyl- $\beta$ -  
383 carboline, and *Paraclostridium sordellii*, which produces turbomycin A and 1,1,1-tris(3-indolyl)-  
384 methane (TIM), are all active against *C. difficile* (36) and could potentiate the toxicity of LCA.  
385 While we attempted to test this hypothesis using the commercially available 1-acetyl- $\beta$ -carboline,  
386 we unfortunately found that *C. difficile* strain 630 $\Delta erm$  is substantially more resistant than the  
387 ATCC 9689 strain used in the study described above (36) (such that solubility limited our ability  
388 to test our hypothesis). Regardless, investigating the interactions between LCA-producing  
389 bacteria and *C. difficile* could reveal that LCA sensing by BapR gives rise to adaptations that  
390 confer a competitive advantage for *C. difficile*.

391         Determining the functions of the other genes repressed by BapR in an LCA-dependent  
392 manner may provide further insight into the function of this MerR family member. Notably, most  
393 MerR family transcription factors sense toxic molecules and upregulate cognate efflux pumps  
394 accordingly. Since *cd3575* is annotated as a sodium:solute symporter and *cd3576* a MFS  
395 transporter, a plausible function of this system is to transport metabolites related to cysteine  
396 catabolism. However, most bile acid-binding transcription factors in bacteria regulate production



397 of multidrug efflux pumps (65–68), and CD3575 and CD3576 could play a role in bile acid efflux.  
398 To date a transporter or channel for bile acids has not been identified in *C. difficile*, but we can  
399 infer this phenomenon from our chemical proteomics screen as the probes were added to intact  
400 cells in culture, washed away, then UV crosslinked. Indeed, many of the hits from our screen are  
401 cytosolic proteins (**Table S1**). A few examples of bacterial bile acid transporters have been  
402 described: the *baiG* gene found in 7 $\alpha$ -dehydroxylating *Clostridium* and *Eubacterium* species  
403 encodes a bile acid transporter (29, 69), *Lactobacillus johnsonii* possesses a bile acid MFS  
404 transporter in conjunction with bile salt hydrolase activity (70), and *Neisseria meningitidis* and  
405 *Yersinia frederiksenii* both have a homologue of the eukaryotic ASBT sodium:bile acid co-  
406 transporter that imports TCA (71–74). *C. difficile* CD3575 and CD3576 share only 11-14% identity  
407 with each of these bile acid transporters, but the possibility remains that they export bile acids.

408         Only a few other bacterial transcription factors have been shown to directly sense bile  
409 acids (65–68), and to our knowledge BapR is the only example that detects bile acids for  
410 metabolic adaptation. While our data are consistent with BapR being a bile acid sensor, *C. difficile*  
411 almost certainly encodes alternative mechanisms for sensing or responding to LCA. Global  
412 transcriptional changes occur in the presence of LCA (**Figure S5**), yet BapR regulates the  
413 expression of only a handful of genes (**Figure 5**). Indeed, our chemical proteomics screen  
414 detected a few other putative transcription factors, two-component system histidine kinases, and  
415 serine/threonine kinases as candidate bile acid-binding proteins with potential signaling roles.  
416 Future studies of these hits could reveal pathways by which *C. difficile* deals with bile acid stress  
417 independent of BapR. For example, while we did not biochemically validate essential hits from  
418 our proteomics screen, inactivation of these proteins by LCA could explain its toxicity. Thus, it  
419 remains to be seen which are involved and whether the toxicity is due to the concerted inactivation  
420 of multiple proteins. Additional studies using bile acid photoaffinity probes and chemical  
421 proteomics should reveal other protein targets and mechanisms of action for these prominent gut  
422 microbiota metabolites.

423

## 424 **Materials and Methods**

### 425 **Bacterial strains and growth conditions.**

426 *C. difficile* strains are of the 630 $\Delta$ *erm* background and mutants were constructed using *pyrE*-  
427 based allele-coupled exchange (54). Strains were grown on brain heart infusion medium  
428 supplemented with 0.5% w/v yeast extract and 0.1% w/v L-cysteine (BHIS) with taurocholate  
429 (TCA; 0.1% w/v; 1.9 mM), thiamphenicol (10–15  $\mu$ g/mL), kanamycin (50  $\mu$ g/mL), or cefoxitin (8  
430  $\mu$ g/mL) as needed. *C. difficile* defined medium (CDDM) (77) was supplemented with 5-fluoroorotic  
431 acid at 2 mg/mL and uracil at 5  $\mu$ g/mL. Cultures were grown swirling at 37°C under anaerobic  
432 conditions using a gas mixture containing 85% N<sub>2</sub>, 5% CO<sub>2</sub> and 10% H<sub>2</sub>. *Escherichia coli* strains  
433 were grown at 37°C with shaking at 225 rpm in Luria-Bertani medium (LB) or at 20°C with shaking  
434 at 225 rpm in autoinduction broth (Terrific broth [Thermo Fisher] with 0.5% glycerol, 0.05%  
435 glucose, and 0.1%  $\alpha$ -lactose monohydrate). Media were supplemented with chloramphenicol (20  
436  $\mu$ g/mL), ampicillin (100  $\mu$ g/mL), or kanamycin (30  $\mu$ g/mL) as needed.

437

### 438 ***C. difficile* growth curves.**

439 *C. difficile* cultures were grown for 3 hours, back-diluted 1:50, and grown for an additional 3 hours  
440 to an OD<sub>600</sub> of ~0.3. Cultures were diluted to an OD<sub>600</sub> of 0.05 and added to 96-well plates with  
441 2X pre-reduced bile acids or probes in BHIS for a total volume of 150  $\mu$ L/well (75  $\mu$ L culture + 75  
442  $\mu$ L 2X compound in BHIS). OD<sub>600</sub> was read every 10 minutes for 18 hours with constant shaking  
443 at 37°C in an Epoch 2 plate reader (BioTek) in an anaerobic chamber. Percent growth inhibition  
444 was calculated from the OD<sub>600</sub> relative to DMSO at 5 hours. Two biological replicates from  
445 independent starter cultures were used per experiment.

446

### 447 **In-gel fluorescent bile acid probe labeling.**

448 *C. difficile* cultures were grown for 3 hours, back-diluted 1:25 into 25 mL BHIS, and grown for an  
449 additional 3-4 hours to an OD<sub>600</sub> of ~0.7. Bile acid probes or DMSO were added to the cultures  
450 and incubated for 30 minutes. Cells were resuspended in 1 mL PBS, transferred to a 24-well plate,  
451 and UV irradiated (365 nm) uncovered for 5 minutes on ice 3-5 cm from the lamp. Probe-  
452 crosslinked cells were pelleted, resuspended in 500 µL cold lysis buffer (1X Halt protease inhibitor  
453 [Thermo Fisher], 0.5 mg/mL lysozyme, 1:1000 benzonase [EMD Millipore], and 0.1% NP-40 in  
454 1X PBS). Cells were lysed by four 30-second rounds of bead beating at speed 6 with Lysing  
455 Matrix B (MP Bio) in a Fast Prep-24 bead beater (MP Bio). Beads were pelleted at 3,000g for 2  
456 minutes and the total lysate was collected. Alexa Fluor 488 was conjugated to the probe in 30 µg  
457 total lysate using a Click-iT Plus Alexa Fluor 488 Picoyl Azide Toolkit (Thermo Fisher). Protein  
458 was precipitated overnight at -20°C in methanol, washed twice with cold methanol, and  
459 resuspended in 25 µL SDS-PAGE sample buffer. Fluorescent probe labeling was visualized in-  
460 gel following SDS-PAGE using the SYBR Safe long pass blue filter in a Fujifilm FLA-9000 imager  
461 at 200 µM resolution. The gel was Coomassie stained as a loading control.

462

#### 463 **Chemical proteomics.**

464 *C. difficile* overnight cultures were diluted 1:25 into 20 mL BHIS and grown to an OD<sub>600</sub> of 1.1.  
465 Bile acid probes or DMSO were added at 10 µM for 1 hour. Cells were resuspended in 1 mL  
466 phosphate-buffered solution (PBS), transferred to a 24-well plate, and UV irradiated (365 nm)  
467 uncovered for 5 minutes on ice 3-5 cm from the lamp. Probe-crosslinked cells were pelleted,  
468 resuspended in 500 µL cold lysis buffer (1X Halt protease inhibitor [Thermo Fisher], 0.5 mg/mL  
469 lysozyme, 1:1000 benzonase [EMD Millipore], and 0.1% NP-40 in 1X PBS). Cells were lysed by  
470 four 30-second rounds of bead beating at speed 6 with Lysing Matrix B (MP Bio) in a Fast Prep-  
471 24 bead beater (MP Bio). Beads were pelleted at 3,000 g for 2 minutes and the total lysate was  
472 collected. The lysate was flash-frozen in liquid nitrogen before further processing. Cell lysates  
473 were centrifuged at 16000 g for 20 min to remove cell debris and supernatants were collected.

474 Each total cell lysates was added with 100  $\mu$ L of click chemistry reagents as a 10X master mix  
475 (az-Biotin: 0.1 mM, 10 mM stock solution in DMSO; tris(2-carboxyethyl)phosphine hydrochloride  
476 (TCEP): 1 mM, 50 mM freshly prepared stock solution in dH<sub>2</sub>O; tris[(1-benzyl-1H-1,2,3-triazol-4-  
477 yl)methyl]amine (TBTA): (0.1 mM, 2 mM stock in 4:1 *t*-butanol: DMSO); CuSO<sub>4</sub> (1 mM, 50 mM  
478 freshly prepared stock in dH<sub>2</sub>O). Samples were mixed well and incubated at room temperature  
479 for 1 h. After incubation, samples were mixed with 4 mL cold methanol and incubated at -20 °C  
480 overnight. Protein pellets were centrifuged at 5000 g for 30 min at 4°C, pellets were transferred  
481 to 2.0 mL centrifuge tube and were washed with 1 mL cold methanol 3 times. After last wash,  
482 pellets were let air dried before being re-solubilized in 250  $\mu$ L 4% SDS PBS with bath sonication.  
483 Solutions were diluted with 750  $\mu$ L PBS, and incubated with 100  $\mu$ L PBS-T-washed High Capacity  
484 NeutrAvidin agarose (Pierce) (500  $\mu$ L PBS-T-washed twice, 2500 g for 60 s) at room temperature  
485 for 1 h with end-to-end rotation. The agarose was washed with 500  $\mu$ L 1% SDS PBS 3 times, 500  
486  $\mu$ L 1M Urea PBS 3 times, and 500  $\mu$ L PBS, 3 times and then reduced with 500  $\mu$ L 10 mM DTT  
487 (Sigma) in PBS for 30 min at 37 °C, and alkylated with 500  $\mu$ L 50 mM iodoacetamide (Sigma) in  
488 PBS for 30 min in dark. 50  $\mu$ L NH<sub>4</sub>HCO<sub>3</sub> (10 mM) was added to the tube. Neutraavidin-bound  
489 proteins were digested on bead with 400 ng Trypsin/Lys-C mix (Promega) at 37 °C overnight with  
490 shaking. Digested peptides were collected (2500 g for 60 s) and lyophilized before being desalted  
491 with custom-made stage-tip containing Empore SPE Extraction Disk (3M). Peptides were eluted  
492 with 2% acetonitrile, 2% formic acid in dH<sub>2</sub>O.

493  
494 Peptide LC-MS analysis was performed with a Dionex 3000 nano-HPLC coupled to an Orbitrap  
495 XL mass spectrometer (Thermo Fisher). Peptide samples were pressure-loaded onto a home-  
496 made C18 reverse-phase column (75  $\mu$ m diameter, 15 cm length). A 180-minute gradient  
497 increasing from 95% buffer A (HPLC grade water with 0.1% formic acid) and 5% buffer B (HPLC  
498 grade acetonitrile with 0.1% formic acid) to 75% buffer B in 133 minutes was used at 200 nL/min.  
499 The Orbitrap XL was operated in top-8-CID-mode with MS spectra measured at a resolution of

500 60,000@m/z 400. One full MS scan (300–2000 MW) was followed by three data-dependent scans  
501 of the most intense ions with dynamic exclusion enabled. Label-free quantification of bile acid  
502 probe-labeled proteins was performed in MaxQuant software as described (78). The search  
503 results from MaxQuant were analyzed by Perseus (<http://www.perseusframework.org/>). Briefly,  
504 the DMSO and bile acid probe-labeled replicates were grouped correspondingly. The results were  
505 cleaned to filter off reverse hits and contaminants. Only proteins that were identified in 3 out of 4  
506 sample replicates and with more than two unique peptides were subjected to subsequent  
507 statistical analysis. LFQ intensities were used for measuring protein abundance and logarithmized  
508 (base 2). Signals that were originally zero were imputed with random numbers from a normal  
509 distribution, whose mean and standard deviation were chosen to best simulate low abundance  
510 values below the noise level (Normal distribution: Width = 0.3; Shift = 1.8).

511

#### 512 **Bile acid probe pull-downs of BapR.**

513 *C. difficile* cultures were grown for 4 hours, back-diluted 1:2,000 into 70 mL BHIS, and grown  
514 overnight. Cultures were then diluted to an OD<sub>600</sub> of 1, split into 20 mL/condition and incubated  
515 with probe or DMSO for 1 hour. Cells were resuspended in 1 mL PBS, transferred to a 6-well  
516 plate, and UV irradiated (365 nm) uncovered for 5 minutes on ice 3-5 cm from the lamp. Probe-  
517 crosslinked cells were pelleted, resuspended in 1 mL cold lysis buffer (1X Halt protease inhibitor  
518 [Thermo Fisher], 0.5 mg/mL lysozyme, 1:1000 benzonase [EMD Millipore], and 0.1% NP-40 in  
519 1X PBS). Cells were lysed by four 30-second rounds of bead beating at speed 6 with Lysing  
520 Matrix B (MP Bio) in a Fast Prep-24 bead beater (MP Bio). Beads were pelleted at 21,000g for 5  
521 minutes at 4°C and the cleared lysate was collected. Biotin was conjugated to the probes in a  
522 click reaction with 0.4 mg cleared lysate in 180 µL PBS and 20 µL 10X click master mix (1 mM  
523 azido-PEG3-biotin [Alfa Aesar], 10 mM tris(2-carboxyethyl)phosphine hydrochloride, 1 mM tris[(1-  
524 benzyl-1H-1,2,3-triazol-4-yl)methyl]amine in 4:1 t-butanol:DMSO, and 10 mM copper sulfate  
525 pentahydrate) and protein was precipitated overnight at -20°C in methanol. Precipitates were

526 washed twice with cold methanol, dried at 37°C for 1 hour, and resolubilized in 50 µL 4% sodium  
527 dodecyl sulfate (SDS) in PBS with bath sonication. 150 µL PBS was added and a sample was  
528 taken as input before incubation with PBS+0.1% Tween-20-washed Pierce High Capacity  
529 NeutrAvidin agarose beads (Thermo Fisher) for 1 hour at room temperature with end-over-end  
530 rotation. Beads were washed three times each with PBS+1% SDS, PBS+4M urea, then PBS and  
531 boiled to elute biotin-probe-protein complexes.

532

### 533 **Recombinant BapR purification.**

534 BL21(DE3) *E. coli* encoding lactose-inducible *bapR* with a C-terminal autoprocessing CPD-His  
535 tag was grown in 20 mL LB with ampicillin, then back-diluted 1:1,000 into 1L autoinduction broth  
536 with ampicillin and grown at 20°C for ~60 hours. Cultures were pelleted, resuspended in 50 mL  
537 low imidazole buffer (LIB; 500 mM NaCl, 50 mM Tris-HCl pH 7.5, 15 mM imidazole, 10% glycerol,  
538 2 mM β-mercaptoethanol), and flash frozen in liquid nitrogen. Once thawed, cells were probe  
539 sonicated (Branson) in 3 x 45 second rounds at 40% amplitude with 5 minutes on ice between.  
540 Lysates were cleared by centrifugation at 13,000 rpm for 45 min at 4°C. BapR-CPD-His was  
541 affinity purified from cleared lysates using Ni-NTA agarose beads (Qiagen) with gentle rocking at  
542 4°C for 2 hours. The beads were washed three times with LIB before inducing cleavage of the  
543 CPD tag (79) with 200 µM inositol hexakisphosphate in LIB at 4°C overnight to elute untagged  
544 BapR. The eluted protein was buffer-exchanged into SEC buffer (200 mM NaCl, 10 mM Tris-HCl  
545 pH 7.5, 5% glycerol, and 1 mM dithiothreitol) and concentrated using an Amicon Ultra-15 10 kDa  
546 cutoff centrifugal filter (Millipore Sigma). Affinity-purified protein was further purified by size  
547 exclusion chromatography (SEC) using a Superdex 200 Increase 10/300 GL column (GE) on an  
548 AKTA Pure fast protein liquid chromatography instrument (GE), reconcentrated, and flash frozen  
549 in aliquots.

550

### 551 **Thermal shift assays.**

552 Affinity- and SEC-purified BapR was added to a mix of 5X SYPRO Orange dye (Thermo Fisher)  
553 and the indicated concentrations of bile acids or DMSO in 1.5X PBS to a final concentration of 1  
554  $\mu$ M in a 96-well white bottom plate. Fluorescence was measured as temperature increased  
555 1°C/minute from 25°C to 95°C in a StepOne Plus qPCR instrument (Applied Biosystems). Protein  
556 from 2 independent purifications was used, and a no-protein control for each ligand at each  
557 concentration was used to identify cutoffs above which the ligand generated background  
558 fluorescence, if at all.

559

### 560 **Phase-contrast microscopy.**

561 *C. difficile* was inoculated into BHIS cultures and grown for 3 hours, back-diluted 1:50, and grown  
562 for another 3 hours. Cultures were then split and treated with DMSO or bile acids at the indicated  
563 concentrations for 3 hours. Aliquots of the cultures were pelleted, resuspended in ~20  $\mu$ L PBS,  
564 and 1  $\mu$ L was spotted on a 1% agarose pad poured in a Gene Frame (Thermo Fisher). Pads were  
565 sealed with a coverslip inside the anaerobic chamber. Phase images were acquired on a Zeiss  
566 Axioskop using a 100X Plan-NEOFLUAR oil phase objective. Cell length was measured from  
567 pole-to-pole using Fiji software and at least 460 cells were measured per strain/condition in 5  
568 independent experiments.

569

### 570 **BapR protein induction by bile acids in *C. difficile*.**

571 *C. difficile* starter cultures were grown for 3 hours, back-diluted 1:50 into 30 mL BHIS, and grown  
572 for an additional 3 hours before being split into new tubes with the indicated concentrations of bile  
573 acids or DMSO. After 3 hours cells were pelleted, resuspended in sample loading buffer, frozen  
574 at -20C, and boiled before running SDS-PAGE. Protein was transferred to a PVDF membrane,  
575 blocked with 0.5X blocking buffer (LI-COR), and probed with chicken  $\alpha$ -GDH antibody (Thermo  
576 Fisher) and a custom mouse  $\alpha$ -BapR antibody (Cocalico Biologicals). Antibodies were detected  
577 using IRDye700- or IRDye800-conjugated donkey  $\alpha$ -chicken and goat  $\alpha$ -mouse secondary

578 antibodies (LI-COR). The blots were imaged using a LI-COR Odyssey CLx imager and quantified  
579 using ImageStudio Lite software (LI-COR).

580

#### 581 **RNA extraction, RNA-seq, and qRT-PCR.**

582 *C. difficile* cultures were grown for 3-4 hours, back-diluted 1:50, and grown for an additional 3-4  
583 hours before being split for treatment with DMSO or 20  $\mu$ M LCA. After 1 or 3 hours of LCA  
584 exposure (OD<sub>600</sub> of 0.1-0.2 at 1 hour or 0.2-0.5 at 3 hours) RNA was extracted using a FastRNA  
585 Pro Blue kit (MP Bio). Samples were treated twice for 45 minutes at 37°C with DNase I (New  
586 England Biolabs) with heat inactivation at 75°C for 10 minutes and DNA was further removed  
587 using a RNeasy Mini kit (Qiagen). RNA was harvested from three independent cultures as  
588 biological replicates per experiment, and independent extractions were used for RNA-seq and  
589 qRT-PCR validation.

590 For RNA-seq analysis an Agilent Bioanalyzer was used to verify RNA quality before  
591 depleting rRNA and ligating adapters and indexes using a Stranded Total RNA with RiboZero  
592 Plus library preparation kit (Illumina). Samples were sequenced as single-end 75 reads on an  
593 Illumina NextSeq 500 sequencer at the Tufts University Genomics Core Facility. Sequences were  
594 trimmed using BBDuk, mapped to the *C. difficile* 630 genome, and analyzed for differential  
595 expression using DESeq2 in Geneious Prime software. Gene functional characterization was  
596 done using GSEA-Pro v3 (University of Groningen) to classify by COG terms and manual  
597 classification for genes that were not classified by GSEA-Pro.

598 For qRT-PCR analysis an Ambion Microbe Express kit (Invitrogen) was used to enrich  
599 mRNA. cDNA was synthesized using a SuperScript First Strand Synthesis kit (Invitrogen). qPCR  
600 was performed using Luna Universal qPCR Master Mix (New England Biolabs) with 1:5 diluted  
601 cDNA in technical duplicate in a StepOne Plus qPCR instrument (Applied Biosystems). A  
602 standard curve made from plasmid encoding the gene of interest or a purified PCR product was  
603 used to enumerate gene copies in each sample. A no-RT control sample was used to ensure no



604 DNA contamination. Primers were designed using the Integrated DNA Technologies Primer Quest  
605 tool.

606

### 607 **Electrophoretic mobility shift assays (EMSAs).**

608 Unlabeled DNA fragments (200-250 bp) encompassing putative promoter regions were amplified  
609 from purified *C. difficile* 630 $\Delta$ *erm* genomic DNA, purified with a GeneJet gel extraction kit (Thermo  
610 Fisher), and used as cold competitors or as templates for PCR with IRDye800-conjugated primers  
611 (Integrated DNA Technologies). The labeled DNA fragments were purified with a GeneJet PCR  
612 purification kit (Thermo Fisher). 20 fmol labeled DNA (or 20 fmol labeled with 1,000 fmol unlabeled  
613 for cold competitor control) was mixed with purified BapR and DMSO or 1  $\mu$ M LCA in binding  
614 buffer (20 mM Tris-HCl pH 8, 10 mM KCl, 2 mM MgCl<sub>2</sub>, 0.5 mM EDTA, 1 mM DTT, 0.05% Nonidet-  
615 P40, 12% v/v glycerol, 25  $\mu$ g/mL salmon sperm DNA) for 20 minutes at room temperature and  
616 run on a 8% native polyacrylamide gel at 225V at 4°C in the dark. DNA was visualized using an  
617 Odyssey CLx imager (LI-COR).

618

### 619 **Data visualization and statistics.**

620 All graphs were generated using Prism 9 software (GraphPad). Chemical structures were  
621 generated using ChemDraw 20.0 software (Perkin Elmer). Statistical analyses were done using  
622 Prism 9 software (GraphPad).

623

624

625 **References**

- 626 1. Abt MC, McKenney PT, Pamer EG. 2016. *Clostridium difficile* colitis: pathogenesis and  
627 host defence. Nat Rev Microbiol 14:609–620.
- 628 2. Rupnik M, Wilcox MH, Gerding DN. 2009. *Clostridium difficile* infection: new developments  
629 in epidemiology and pathogenesis. 7. Nat Rev Microbiol 7:526–536.
- 630 3. Guh AY, Mu Y, Winston LG, Johnston H, Olson D, Farley MM, Wilson LE, Holzbauer SM,  
631 Phipps EC, Dumyati GK, Beldavs ZG, Kainer MA, Karlsson M, Gerding DN, McDonald LC.  
632 2020. Trends in U.S. Burden of *Clostridioides difficile* Infection and Outcomes. New Engl J  
633 Med.
- 634 4. Koenigskecht MJ, Theriot CM, Bergin IL, Schumacher CA, Schloss PD, Young VB. 2015.  
635 Dynamics and establishment of *Clostridium difficile* infection in the murine gastrointestinal  
636 tract. Infect Immun 83:934–941.
- 637 5. Theriot CM, Koenigskecht MJ, Carlson PE, Hatton GE, Nelson AM, Li B, Huffnagle GB, Z  
638 Li J, Young VB. 2014. Antibiotic-induced shifts in the mouse gut microbiome and  
639 metabolome increase susceptibility to *Clostridium difficile* infection. Nat Commun 5:3114.
- 640 6. Theriot CM, Bowman AA, Young VB. 2016. Antibiotic-Induced Alterations of the Gut  
641 Microbiota Alter Secondary Bile Acid Production and Allow for *Clostridium difficile* Spore  
642 Germination and Outgrowth in the Large Intestine. mSphere 1.
- 643 7. Buffie CG, Bucci V, Stein RR, McKenney PT, Ling L, Gobourne A, No D, Liu H, Kinnebrew  
644 M, Viale A, Littmann E, van den Brink MRM, Jenq RR, Taur Y, Sander C, Cross JR,  
645 Toussaint NC, Xavier JB, Pamer EG. 2015. Precision microbiome reconstitution restores  
646 bile acid mediated resistance to *Clostridium difficile*. Nature 517:205–208.

- 647 8. Weingarden AR, Chen C, Bobr A, Yao D, Lu Y, Nelson VM, Sadowsky MJ, Khoruts A.  
648 2014. Microbiota transplantation restores normal fecal bile acid composition in recurrent  
649 *Clostridium difficile* infection. Am J Physiol Gastrointest Liver Physiol 306:G310–G319.
- 650 9. Sato Y, Atarashi K, Plichta DR, Arai Y, Sasajima S, Kearney SM, Suda W, Takeshita K,  
651 Sasaki T, Okamoto S, Skelly AN, Okamura Y, Vlamakis H, Li Y, Tanoue T, Takei H,  
652 Nittono H, Narushima S, Irie J, Itoh H, Moriya K, Sugiura Y, Suematsu M, Moritoki N,  
653 Shibata S, Littman DR, Fischbach MA, Uwamino Y, Inoue T, Honda A, Hattori M, Murai T,  
654 Xavier RJ, Hirose N, Honda K. 2021. Novel bile acid biosynthetic pathways are enriched in  
655 the microbiome of centenarians. Nature 599:458–464.
- 656 10. Ridlon JM, Kang D-J, Hylemon PB. 2006. Bile salt biotransformations by human intestinal  
657 bacteria. J Lipid Res 47:241–259.
- 658 11. Hamilton JP, Xie G, Raufman J-P, Hogan S, Griffin TL, Packard CA, Chatfield DA, Hagey  
659 LR, Steinbach JH, Hofmann AF. 2007. Human cecal bile acids: concentration and  
660 spectrum. Amer J Physiol Gastrointest Liver Physiol 293:G256–G263.
- 661 12. Yoshimoto S, Loo TM, Atarashi K, Kanda H, Sato S, Oyadomari S, Iwakura Y, Oshima K,  
662 Morita H, Hattori M, Hattori M, Honda K, Ishikawa Y, Hara E, Ohtani N. 2013. Obesity-  
663 induced gut microbial metabolite promotes liver cancer through senescence secretome.  
664 Nature 499:97–101.
- 665 13. Winston JA, Rivera AJ, Cai J, Thanissery R, Montgomery SA, Patterson AD, Theriot CM.  
666 2020. Ursodeoxycholic Acid (UDCA) Mitigates the Host Inflammatory Response during  
667 *Clostridioides difficile* Infection by Altering Gut Bile Acids. Infect Immun 88:e00045-20.
- 668 14. Ma C, Han M, Heinrich B, Fu Q, Zhang Q, Sandhu M, Agdashian D, Terabe M, Berzofsky  
669 JA, Fako V, Ritz T, Longerich T, Theriot CM, McCulloch JA, Roy S, Yuan W, Thovarai V,

- 670 Sen SK, Ruchirawat M, Korangy F, Wang XW, Trinchieri G, Greten TF. 2018. Gut  
671 microbiome-mediated bile acid metabolism regulates liver cancer via NKT cells. *Science*  
672 360:eaan5931.
- 673 15. Song X, Sun X, Oh SF, Wu M, Zhang Y, Zheng W, Geva-Zatorsky N, Jupp R, Mathis D,  
674 Benoist C, Kasper DL. 2020. Microbial bile acid metabolites modulate gut ROR $\gamma$ +  
675 regulatory T cell homeostasis. *Nature* 577:410–415.
- 676 16. Winkler ES, Shrihari S, Hykes BL, Handley SA, Andhey PS, Huang Y-JS, Swain A, Droit L,  
677 Chebrolu KK, Mack M, Vanlandingham DL, Thackray LB, Cella M, Colonna M, Artyomov  
678 MN, Stappenbeck TS, Diamond MS. 2020. The intestinal microbiome restricts alphavirus  
679 infection and dissemination through a bile acid-type I IFN signaling axis. *Cell* 182:901-  
680 918.e18.
- 681 17. Campbell C, McKenney PT, Konstantinovskiy D, Isaeva OI, Schizas M, Verter J, Mai C, Jin  
682 W-B, Guo C-J, Violante S, Ramos RJ, Cross JR, Kadaveru K, Hambor J, Rudensky AY.  
683 2020. Bacterial metabolism of bile acids promotes generation of peripheral regulatory T  
684 cells. 7809. *Nature* 581:475–479.
- 685 18. Li W, Hang S, Fang Y, Bae S, Zhang Y, Zhang M, Wang G, McCurry MD, Bae M, Paik D,  
686 Franzosa EA, Rastinejad F, Huttenhower C, Yao L, Devlin AS, Huh JR. 2021. A bacterial  
687 bile acid metabolite modulates Treg activity through the nuclear hormone receptor NR4A1.  
688 *Cell Host & Microbe* 29:1366-1377.e9.
- 689 19. Paik D, Yao L, Zhang Y, Bae S, D'Agostino GD, Zhang M, Kim E, Franzosa EA, Avila-  
690 Pacheco J, Bisanz JE, Rakowski CK, Vlamakis H, Xavier RJ, Turnbaugh PJ, Longman RS,  
691 Krout MR, Clish CB, Rastinejad F, Huttenhower C, Huh JR, Devlin AS. 2022. Human gut  
692 bacteria produce TH17-modulating bile acid metabolites. *Nature* 1–6.

- 693 20. Sinha SR, Haileselassie Y, Nguyen LP, Tropini C, Wang M, Becker LS, Sim D, Jarr K,  
694 Spear ET, Singh G, Namkoong H, Bittinger K, Fischbach MA, Sonnenburg JL, Habtezion  
695 A. 2020. Dysbiosis-Induced Secondary Bile Acid Deficiency Promotes Intestinal  
696 Inflammation. *Cell Host & Microbe* 2020.
- 697 21. Grau KR, Zhu S, Peterson ST, Helm EW, Philip D, Phillips M, Hernandez A, Turula H,  
698 Frasse P, Graziano VR, Wilen CB, Wobus CE, Baldrige MT, Karst SM. 2020. Commensal  
699 bacteria regulate regionalization of acute norovirus infection along the intestinal tract  
700 through bile acid-mediated priming of type III interferon. *Nat Microbiol* 5:84–92.
- 701 22. Vidal JE, Wier MN, A Angulo-Zamudio U, McDevitt E, Jop Vidal AG, Alibayov B, Scasny A,  
702 Wong SM, Akerley BJ, McDaniel LS. 2021. Prophylactic Inhibition of Colonization by  
703 *Streptococcus pneumoniae* with the Secondary Bile Acid Metabolite Deoxycholic Acid.  
704 *Infect Immun* 89:e0046321.
- 705 23. Urdaneta V, Casadesús J. 2017. Interactions between Bacteria and Bile Salts in the  
706 Gastrointestinal and Hepatobiliary Tracts. *Front Med (Lausanne)* 4:163.
- 707 24. Ruiz L, Margolles A, Sánchez B. 2013. Bile resistance mechanisms in *Lactobacillus* and  
708 *Bifidobacterium*. *Front Microbiol* 4:396.
- 709 25. Ridlon JM, Kang D-J, Hylemon PB. 2010. Isolation and Characterization of a Bile Acid  
710 Inducible 7 $\alpha$ -dehydroxylating operon in *Clostridium hylemonae* TN271. *Anaerobe* 16:137–  
711 146.
- 712 26. Kang D-J, Ridlon JM, Moore DR, Barnes S, Hylemon PB. 2008. *Clostridium scindens*  
713 *baiCD* and *baiH* genes encode stereo-specific 7 $\alpha$ /7 $\beta$ -hydroxy-3-oxo- $\Delta$ 4-cholenoic acid  
714 oxidoreductases. *Biochim Biophys Acta* 1781:16–25.

- 715 27. Dawson JA, Mallonee DH, Björkhem I, Hylemon PB. 1996. Expression and  
716 characterization of a C24 bile acid 7 alpha-dehydratase from *Eubacterium* sp. strain VPI  
717 12708 in *Escherichia coli*. *Journal of Lipid Research* 37:1258–1267.
- 718 28. Mallonee DH, White WB, Hylemon PB. 1990. Cloning and sequencing of a bile acid-  
719 inducible operon from *Eubacterium* sp. strain VPI 12708. *J Bacteriol* 172:7011–7019.
- 720 29. Wells JE, Hylemon PB. 2000. Identification and Characterization of a Bile Acid 7 $\alpha$ -  
721 Dehydroxylation Operon in *Clostridium* sp. Strain TO-931, a Highly Active 7 $\alpha$ -  
722 Dehydroxylating Strain Isolated from Human Feces. *Appl Environ Microbiol* 66:1107–1113.
- 723 30. Solbach P, Chhatwal P, Woltemate S, Tacconelli E, Buhl M, Gerhard M, Thoeringer CK,  
724 Vehreschild MJGT, Jazmati N, Rupp J, Manns MP, Bachmann O, Suerbaum S. 2018.  
725 *BaiCD* gene cluster abundance is negatively correlated with *Clostridium difficile* infection.  
726 *PLOS ONE* 13:e0196977.
- 727 31. Reed AD, Nethery MA, Stewart A, Barrangou R, Theriot CM. 2020. Strain-Dependent  
728 Inhibition of *Clostridioides difficile* by Commensal Clostridia Carrying the Bile Acid-  
729 Inducible (*bai*) Operon. *J Bacteriol* 202:e00039-20.
- 730 32. Aguirre AM, Yalcinkaya N, Wu Q, Swennes A, Tessier ME, Roberts P, Miyajima F,  
731 Savidge T, Sorg JA. 2021. Bile acid-independent protection against *Clostridioides difficile*  
732 infection. *PLoS Pathog* 17:e1010015.
- 733 33. Studer N, Desharnais L, Beutler M, Brugiroux S, Terrazos MA, Menin L, Schürch CM,  
734 McCoy KD, Kuehne SA, Minton NP, Stecher B, Bernier-Latmani R, Hapfelmeier S. 2016.  
735 Functional Intestinal Bile Acid 7 $\alpha$ -Dehydroxylation by *Clostridium scindens* Associated with  
736 Protection from *Clostridium difficile* Infection in a Gnotobiotic Mouse Model. *Frontiers in*  
737 *Cellular and Infection Microbiology* 6:191.

- 738 34. Weingarden AR, Dosa PI, DeWinter E, Steer CJ, Shaughnessy MK, Johnson JR, Khoruts  
739 A, Sadowsky MJ. 2016. Changes in Colonic Bile Acid Composition following Fecal  
740 Microbiota Transplantation Are Sufficient to Control *Clostridium difficile* Germination and  
741 Growth. PLoS One 11.
- 742 35. Lewis BB, Carter RA, Pamer EG. 2016. Bile acid sensitivity and in vivo virulence of clinical  
743 *Clostridium difficile* isolates. Anaerobe 41:32–36.
- 744 36. Kang JD, Myers CJ, Harris SC, Kakiyama G, Lee I-K, Yun B-S, Matsuzaki K, Furukawa M,  
745 Min H-K, Bajaj JS, Zhou H, Hylemon PB. 2019. Bile Acid 7 $\alpha$ -Dehydroxylating Gut Bacteria  
746 Secrete Antibiotics that Inhibit *Clostridium difficile*: Role of Secondary Bile Acids. Cell  
747 Chemical Biology 26:27-34.e4.
- 748 37. Sistrunk JR, Nickerson KP, Chanin RB, Rasko DA, Faherty CS. 2016. Survival of the  
749 Fittest: How Bacterial Pathogens Utilize Bile To Enhance Infection. Clinical Microbiology  
750 Reviews 29:819–836.
- 751 38. Sievers S, Metzendorf NG, Dittmann S, Troitzsch D, Gast V, Tröger SM, Wolff C, Zühlke  
752 D, Hirschfeld C, Schlüter R, Riedel K. 2019. Differential View on the Bile Acid Stress  
753 Response of *Clostridioides difficile*. Front Microbiol 10:258.
- 754 39. Dubois T, Tremblay YDN, Hamiot A, Martin-Verstraete I, Deschamps J, Monot M, Briandet  
755 R, Dupuy B. 2019. A microbiota-generated bile salt induces biofilm formation in *Clostridium*  
756 *difficile*. NPJ Biofilms Microbiomes 5.
- 757 40. Tam J, Icho S, Utama E, Orrell KE, Gómez-Biagi RF, Theriot CM, Kroh HK, Rutherford SA,  
758 Lacy DB, Melnyk RA. 2020. Intestinal bile acids directly modulate the structure and  
759 function of *C. difficile* TcdB toxin. Proc Natl Acad Sci USA 117:6792–6800.

- 760 41. Thanissery R, Winston JA, Theriot CM. 2017. Inhibition of spore germination, growth, and  
761 toxin activity of clinically relevant *C. difficile* strains by gut microbiota derived secondary  
762 bile acids. *Anaerobe* 45:86–100.
- 763 42. Francis MB, Allen CA, Shrestha R, Sorg JA. 2013. Bile Acid Recognition by the *Clostridium*  
764 *difficile* Germinant Receptor, CspC, Is Important for Establishing Infection. *PLoS*  
765 *Pathogens* 9:e1003356.
- 766 43. Sorg JA, Sonenshein AL. 2008. Bile salts and glycine as cogermnants for *Clostridium*  
767 *difficile* spores. *J Bacteriol* 190:2505–12.
- 768 44. Parasar B, Zhou H, Xiao X, Shi Q, Brito IL, Chang PV. 2019. Chemoproteomic Profiling of  
769 Gut Microbiota-Associated Bile Salt Hydrolase Activity. *ACS Cent Sci* 5:867–873.
- 770 45. Dembek M, Barquist L, Boinett CJ, Cain AK, Mayho M, Lawley TD, Fairweather NF, Fagan  
771 RP. 2015. High-throughput analysis of gene essentiality and sporulation in *Clostridium*  
772 *difficile*. *mBio* 6:e02383.
- 773 46. Schumacher MA, Brennan RG. 2002. Structural mechanisms of multidrug recognition and  
774 regulation by bacterial multidrug transcription factors. *Mol Microbiol* 45:885–893.
- 775 47. Roy A, Kucukural A, Zhang Y. 2010. I-TASSER: a unified platform for automated protein  
776 structure and function prediction. *Nat Protoc* 5:725–738.
- 777 48. Brown NL, Stoyanov JV, Kidd SP, Hobman JL. 2003. The MerR family of transcriptional  
778 regulators. *FEMS Microbiology Reviews* 27:145–163.
- 779 49. Markham PN, Loguidice J, Neyfakh AA. 1997. Broad Ligand Specificity of the  
780 Transcriptional Regulator of the *Bacillus subtilis* Multidrug Transporter Bmr. *Biochem*  
781 *Biophys Res Comm* 239:269–272.



- 782 50. Vázquez-Laslop N, Markham PN, Neyfakh AA. 1999. Mechanism of Ligand Recognition by  
783 BmrR, the Multidrug-Responding Transcriptional Regulator: Mutational Analysis of the  
784 Ligand-Binding Site. *Biochemistry* 38:16925–16931.
- 785 51. Heldwein EEZ, Brennan RG. 2001. Crystal structure of the transcription activator BmrR  
786 bound to DNA and a drug. 6818. *Nature* 409:378–382.
- 787 52. Hamiaux C, Drummond RSM, Janssen BJ, Ledger SE, Cooney JM, Newcomb RD,  
788 Snowden KC. 2012. DAD2 Is an  $\alpha/\beta$  Hydrolase Likely to Be Involved in the Perception of  
789 the Plant Branching Hormone, Strigolactone. *Curr Biol* 22:2032–2036.
- 790 53. Kabir A, Honda RP, Kamatari YO, Endo S, Fukuoka M, Kuwata K. 2016. Effects of ligand  
791 binding on the stability of aldo–keto reductases: Implications for stabilizer or destabilizer  
792 chaperones. *Prot Sci* 25:2132–2141.
- 793 54. Ng YK, Ehsaan M, Philip S, Collery MM, Janoir C, Collignon A, Cartman ST, Minton NP.  
794 2013. Expanding the Repertoire of Gene Tools for Precise Manipulation of the *Clostridium*  
795 *difficile* Genome: Allelic Exchange Using *pyrE* Alleles. *PLoS ONE* 8.
- 796 55. Dubois T, Dancer-Thibonnier M, Monot M, Hamiot A, Bouillaut L, Soutourina O, Martin-  
797 Verstraete I, Dupuy B. 2016. Control of *Clostridium difficile* Physiopathology in Response  
798 to Cysteine Availability. *Infect Immun* 84:2389–2405.
- 799 56. Soutourina O, Dubois T, Monot M, Shelyakin PV, Saujet L, Boudry P, Gelfand MS, Dupuy  
800 B, Martin-Verstraete I. 2020. Genome-Wide Transcription Start Site Mapping and Promoter  
801 Assignments to a Sigma Factor in the Human Enteropathogen *Clostridioides difficile*. *Front*  
802 *Microbiol* 11.

- 803 57. Reynolds CB, Emerson JE, de la Riva L, Fagan RP, Fairweather NF. 2011. The  
804 *Clostridium difficile* Cell Wall Protein CwpV is Antigenically Variable between Strains, but  
805 Exhibits Conserved Aggregation-Promoting Function. PLoS Pathog 7:e1002024.
- 806 58. Sekulovic O, Ospina Bedoya M, Fivian-Hughes AS, Fairweather NF, Fortier L. 2015. The  
807 *Clostridium difficile* cell wall protein CwpV confers phase-variable phage resistance. Mol  
808 Microbiol 98:329–342.
- 809 59. Emerson JE, Reynolds CB, Fagan RP, Shaw HA, Goulding D, Fairweather NF. 2009. A  
810 novel genetic switch controls phase variable expression of CwpV, a *Clostridium difficile* cell  
811 wall protein. Mol Microbiol 74:541–556.
- 812 60. Ansari AZ, Bradner JE, O’Halloran TV. 1995. DNA-bend modulation in a repressor-to-  
813 activator switching mechanism. Nature 374:371–375.
- 814 61. Outten CE, Outten FW, O’Halloran TV. 1999. DNA distortion mechanism for transcriptional  
815 activation by ZntR, a Zn(II)-responsive MerR homologue in Escherichia coli. J Biol Chem  
816 274:37517–37524.
- 817 62. Philips SJ, Canalizo-Hernandez M, Yildirim I, Schatz GC, Mondragón A, O’Halloran TV.  
818 2015. Allosteric Transcriptional Regulation via changes in the Overall Topology of the Core  
819 Promoter. Science 349:877–881.
- 820 63. Shewchuk LM, Helmann JD, Ross W, Park SJ, Summers AO, Walsh CT. 1989.  
821 Transcriptional switching by the MerR protein: activation and repression mutants implicate  
822 distinct DNA and mercury(II) binding domains. Biochemistry 28:2340–2344.

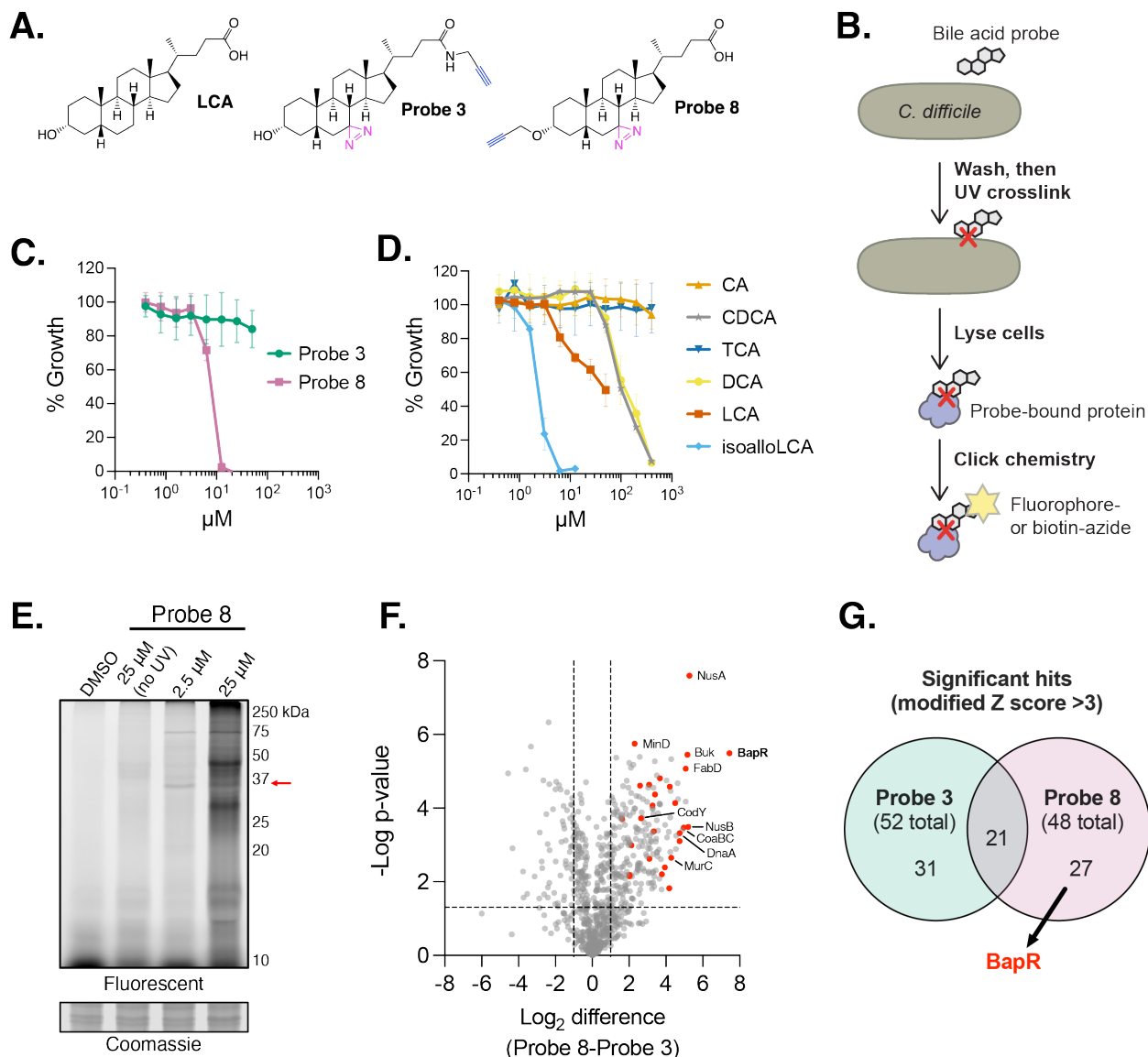
- 823 64. Chang C-C, Lin L-Y, Zou X-W, Huang C-C, Chan N-L. 2015. Structural basis of the  
824 mercury(II)-mediated conformational switching of the dual-function transcriptional regulator  
825 MerR. *Nucleic Acids Res* 43:7612–7623.
- 826 65. Beggs GA, Zalucki YM, Brown NG, Rastegari S, Phillips RK, Palzkill T, Shafer WM,  
827 Kumaraswami M, Brennan RG. 2019. Structural, Biochemical, and In Vivo Characterization  
828 of MtrR-Mediated Resistance to Innate Antimicrobials by the Human Pathogen *Neisseria*  
829 *gonorrhoeae*. *J Bacteriol* 201.
- 830 66. Lei H-T, Shen Z, Surana P, Routh MD, Su C-C, Zhang Q, Yu EW. 2011. Crystal structures  
831 of CmeR-bile acid complexes from *Campylobacter jejuni*. *Prot Sci* 20:712–23.
- 832 67. Quillin SJ, Schwartz KT, Leber JH. 2011. The novel *Listeria monocytogenes* bile sensor  
833 BrtA controls expression of the cholic acid efflux pump MdrT. *Mol Microbiol* 81:129–142.
- 834 68. Nikaido E, Yamaguchi A, Nishino K. 2008. AcrAB multidrug efflux pump regulation in  
835 *Salmonella enterica* serovar Typhimurium by RamA in response to environmental signals.  
836 *J Biol Chem* 283:24245–24253.
- 837 69. Mallonee DH, Hylemon PB. 1996. Sequencing and expression of a gene encoding a bile  
838 acid transporter from *Eubacterium* sp. strain VPI 12708. *J Bacteriol* 178:7053–7058.
- 839 70. Elkins CA, Moser SA, Savage DCY 2001. Genes encoding bile salt hydrolases and  
840 conjugated bile salt transporters in *Lactobacillus johnsonii* 100-100 and other *Lactobacillus*  
841 species. *Microbiology* 147:3403–3412.
- 842 71. Hu N-J, Iwata S, Cameron AD, Drew D. 2011. Crystal structure of a bacterial homologue of  
843 the bile acid sodium symporter ASBT. *Nature* 478:408–411.

- 844 72. Lu P-H, Li C-C, Chiang Y-W, Liu J-H, Chiang WT, Chao Y-H, Li G-S, Weng S-E, Lin S-Y,  
845 Hu N-J. 2021. Dissecting the Conformational Dynamics of the Bile Acid Transporter  
846 Homologue ASBTNM. *J Mol Biol* 433:166764.
- 847 73. Wang X, Lyu Y, Ji Y, Sun Z, Zhou X. 2021. Substrate binding in the bile acid transporter  
848 ASBTYf from *Yersinia frederiksenii*. 1. *Acta Cryst D* 77:117–125.
- 849 74. Zhou X, Levin EJ, Pan Y, McCoy JG, Sharma R, Kloss B, Bruni R, Quick M, Zhou M. 2014.  
850 Structural basis of the alternating-access mechanism in a bile acid transporter. *Nature*  
851 505:569–573.
- 852 75. Lord SJ, Velle KB, Mullins RD, Fritz-Laylin LK. 2020. SuperPlots: Communicating  
853 reproducibility and variability in cell biology. *J Cell Biol* 219:e202001064.
- 854 76. Jenior ML, Leslie JL, Young VB, Schloss PD. *Clostridium difficile* Colonizes Alternative  
855 Nutrient Niches during Infection across Distinct Murine Gut Microbiomes. *mSystems*  
856 2:e00063-17.
- 857 77. Karasawa T, Ikoma S, Yamakawa K, Nakamura S. 1995. A defined growth medium for  
858 *Clostridium difficile*. *Microbiology* 141:371–375.
- 859 78. Cox J, Hein MY, Lubner CA, Paron I, Nagaraj N, Mann M. 2014. Accurate Proteome-wide  
860 Label-free Quantification by Delayed Normalization and Maximal Peptide Ratio Extraction,  
861 Termed MaxLFQ. *Mol Cell Proteomics* 13:2513–2526.
- 862 79. Shen A, Lupardus PJ, Morell M, Ponder EL, Sadaghiani AM, Garcia KC, Bogoy M. 2009.  
863 Simplified, enhanced protein purification using an inducible, autoprocessing enzyme tag.  
864 *PLoS ONE* 4.
- 865

866

867

868



869

870 **Figure 1. Identification of bile acid binding proteins by chemical proteomics. (A)** Structures

871 of bile acid probes; diazine ring for UV crosslinking shown in magenta and terminal alkyne for

872 click chemistry shown in blue. (B) Schematic of bile acid probe labeling and detection. (C)

873 Inhibition of *C. difficile* growth in broth culture across various concentrations of bile acid probes

874 calculated from OD<sub>600</sub> after 5 hours of growth; error bars represent SD, n = 4 in two experiments.

875 (D) Growth inhibition as in (C) with bile acids; error bars represent SD, n = 4 in two experiments.

876 (E) In-gel fluorescent detection of probe labeling as illustrated in (C); cells were treated with probe

877 for 30 minutes during log phase and Coomassie stain serves as a loading control, the gel is

878 representative of three experiments. The red arrow indicates a band approximately the size of

879 BapR. (F) Comparison of proteins isolated from *C. difficile* using Probe 8 vs Probe 3 and identified

880 by LC-MS/MS; cells were grown with 10  $\mu$ M probes for 1 hour during log-phase, dashed lines

881 indicate  $p < 0.05$  or 2-fold LFQ intensity difference and significant hits for Probe 8 (modified Z

882 score  $> 3$ ) are shown in red, n = 3. (G) Comparison of hits in each dataset, BapR is a significant

883 hit for Probe 8 but not Probe 3.

884

885

886

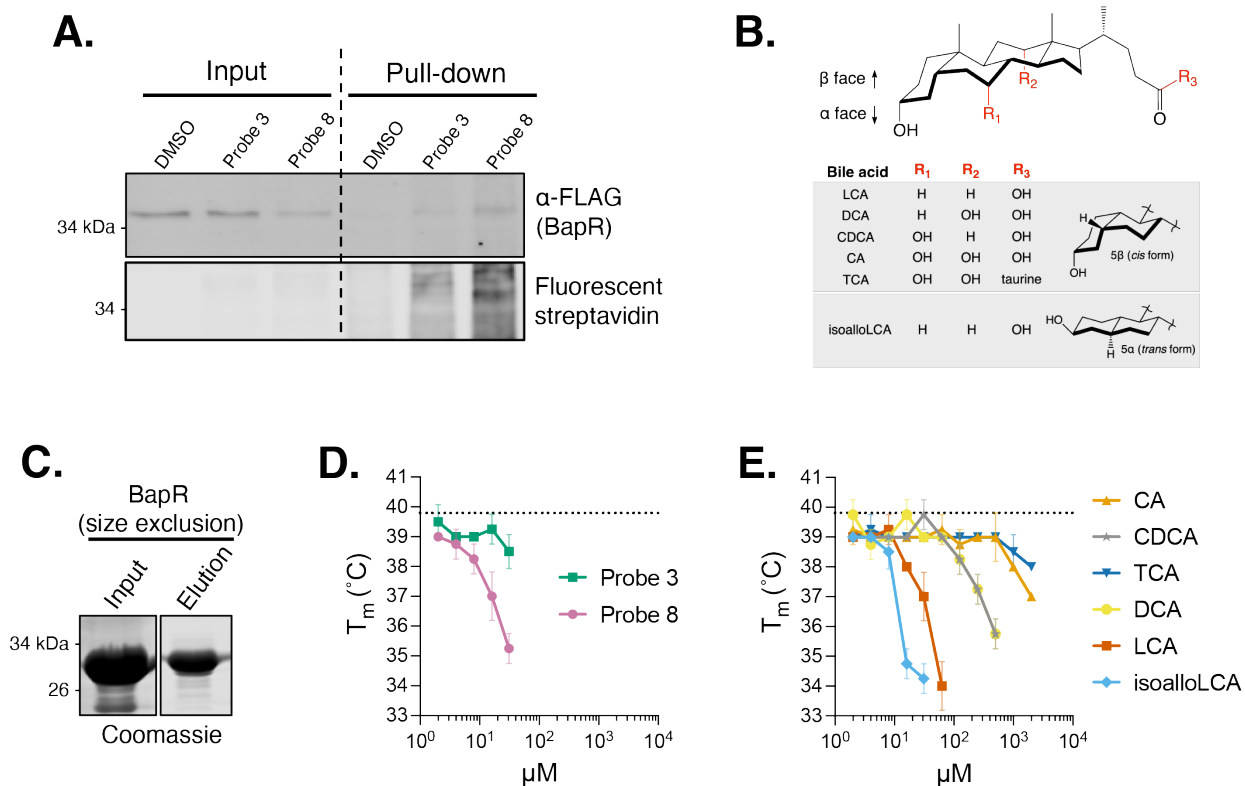
887

888

889

890

891



892

893 **Figure 2. Validation of BapR as a bile acid-binding protein. (A)** Pull-down of BapR from *C.*

894 *difficile* using bile acid probes; cells were treated with 10  $\mu$ M probes for 1 hour during log-phase

895 before following the workflow in Figure 1C with biotin, then streptavidin beads pulled down the

896 probe and BapR if bound. BapR was FLAG-tagged to facilitate its detection. Input samples were

897 taken after the click reaction conjugating biotin to the probe, and fluorescent streptavidin detects

898 presence of the probe. Blot is representative of 3 independent experiments. **(B)** Summarized

899 structures of the bile acids used in this study. **(C)** Size exclusion chromatography of BapR after

900 affinity purification. The gel is representative of 2 independent purifications. **(D)** Thermal shift

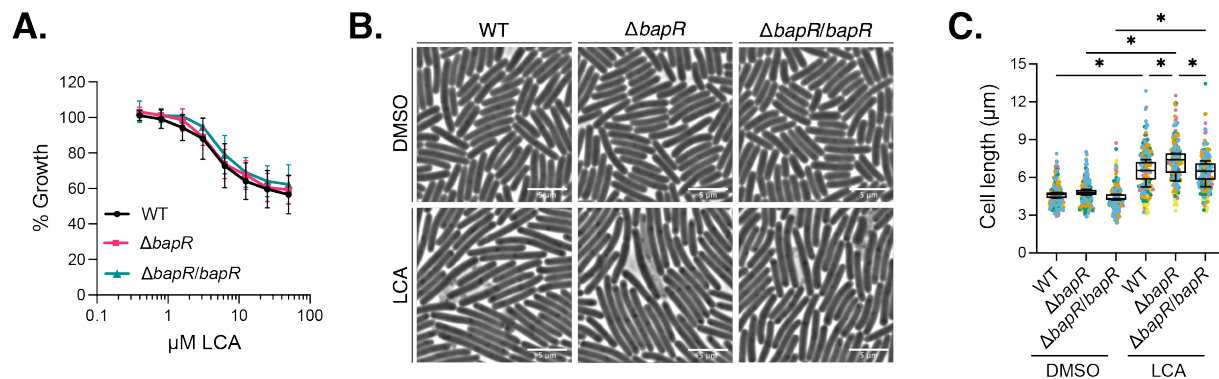
901 assay with purified BapR; the melting temperature ( $T_m$ ) of BapR was assessed using SYPRO

902 Orange dye across a range of bile acid probe concentrations; a change in melting temperature is

903 indicative of binding. Dashed line indicates  $T_m$  of BapR in the presence of DMSO vehicle, error

904 bars represent SD,  $n = 4$  with protein from two independent protein purifications. **(E)** Thermal shift

905 assay as in (D) with bile acids.



906

907 **Figure 3. BapR influences cell length in the presence of LCA. (A)** Inhibition of WT,  $\Delta bapR$ ,

908 and  $\Delta bapR/bapR$  *C. difficile* growth in broth culture across various concentrations of LCA

909 calculated from  $\text{OD}_{600}$  after 5 hours of growth; error bars represent SD,  $n = 2$ . **(B)** Phase-contrast

910 images of wildtype (WT) *C. difficile*,  $\Delta bapR$ , and  $\Delta bapR/bapR$ , the complement strain carrying

911 *bapR* at an ectopic locus after 3-hour treatment with 20  $\mu\text{M}$  LCA or DMSO vehicle during log-

912 phase; images are representative of 5 independent experiments. **(C)** Measurement of cell length

913 from the experiments in (A); at least 460 cells were measured per strain per condition for each

914 experiment and the length of 35 random cells per experiment are shown (75). Colors represent

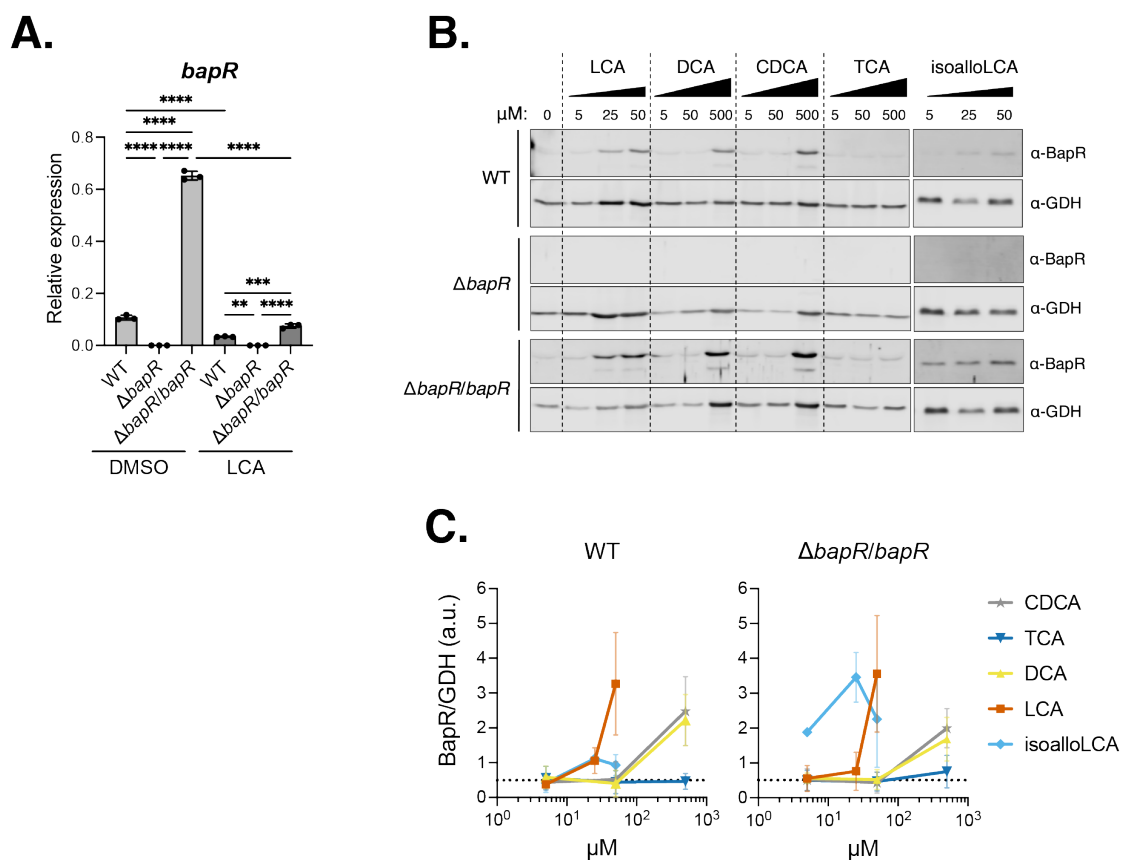
915 independent experiments, \* $p < 0.05$  by repeated measures one-way ANOVA with Tukey

916 correction.

917

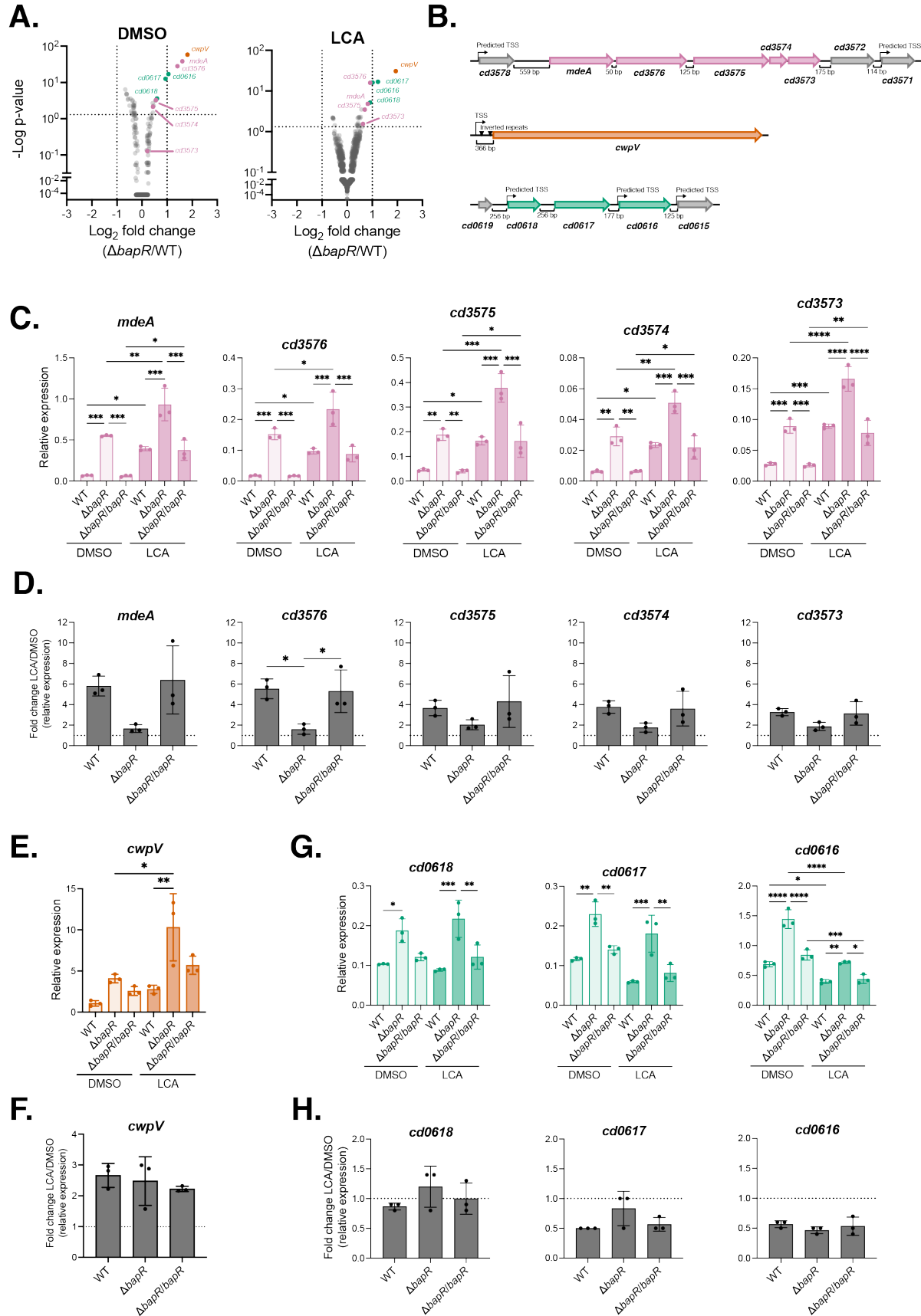
918





919

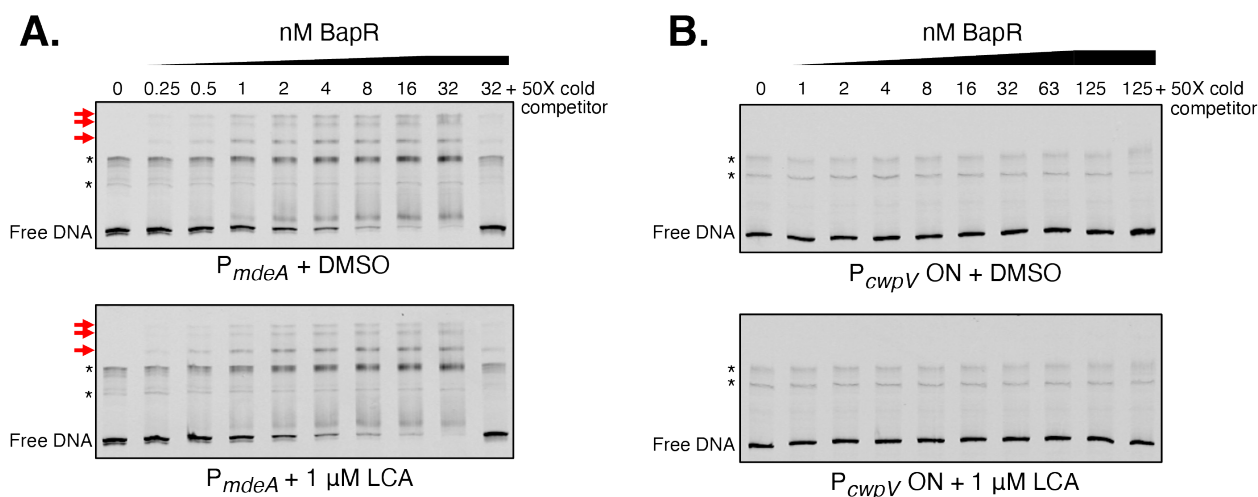
920 **Figure 4. BapR is stabilized by bile acids.** (A) Expression of *bapR* measured by qRT-PCR after  
 921 1-hour exposure to 20  $\mu$ M LCA or DMSO vehicle; expression is relative to the housekeeping  
 922 threonyl-tRNA synthetase *thrS* (76).  $n = 3$ , \*\* $p < 0.01$ , \*\*\* $p < 0.001$ , \*\*\*\* $p < 0.0001$  by one-way  
 923 ANOVA with Tukey correction. (B) Bile acids were added to log-phase *C. difficile* cultures at the  
 924 indicated concentrations and samples were taken after 3 hours for Western blotting; glutamate  
 925 dehydrogenase (GDH) serves as a loading control and blots are representative of 3 biological  
 926 replicates. (C) Quantification of the blots in (A);  $n = 3$ .



928 **Figure 5. Genes regulated by BapR.** (A) RNA-seq analysis of WT and  $\Delta bapR$  *C. difficile* after  
929 1-hour treatment with DMSO vehicle or 20  $\mu$ M LCA during log-phase; dashed lines indicate  
930 significance cutoffs at  $p < 0.05$  and fold change  $> 2$ ,  $n = 3$ . (B) Genomic context of hits from (A).  
931 (C) Expression of the *mdeA* gene cluster measured by qRT-PCR using purified RNA that is  
932 distinct from the 1-hour exposure to DMSO or 20  $\mu$ M LCA used for RNA-seq; expression is relative  
933 to *thrS*,  $n = 3$ . (D) Relative expression data in (C) plotted as fold change LCA over DMSO for each  
934 strain. (E) Expression of *cwpV* as in (C). (F) Fold change LCA/DMSO for *cwpV* as in (D). (G)  
935 Expression of *cd0618* gene cluster as in (C). (H) Fold change LCA/DMSO for *cd0618* gene cluster  
936 as in (D). \* $p < 0.05$ , \*\* $p < 0.01$ , \*\*\* $p < 0.001$ , \*\*\*\* $p < 0.0001$  by one-way ANOVA with Tukey  
937 correction.  
938  
939

940

941



942

943 **Figure 6. BapR directly regulates *mdeA*.** (A) Electrophoretic mobility shift assay with purified

944 BapR and a 250 bp DNA fragment comprising the region immediately upstream of the *mdeA* start

945 codon as a putative promoter; 20 fmol 5' IRDye800-labeled promoter fragment per lane, the last

946 lane contains 20 fmol labeled DNA and 1,000 fmol of the same DNA fragment lacking the

947 fluorescent label as a cold competitor. Gel is representative of 3 replicates with protein from 2

948 independent purifications. "Free DNA" indicates unbound DNA and red arrows indicate BapR-

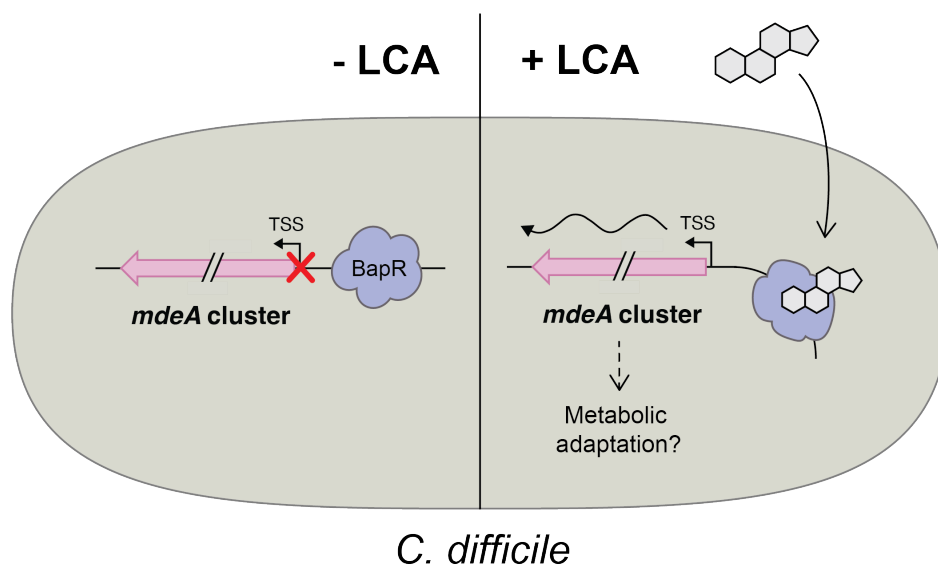
949 bound DNA. Asterisks denote nonspecific bands that likely represent different DNA secondary

950 structures. (B) Assay as in (A) with a 356 bp DNA fragment encompassing the *cwpV* promoter in

951 its "on" orientation.

952

953



954

955

956 **Figure 7. Model of proposed BapR function.** Consistent with MerR family proteins, BapR is  
957 DNA-bound in the absence of LCA and represses gene expression. Upon binding LCA, BapR  
958 changes conformation to reorient the promoter and allow transcription, possibly for the purpose  
959 of metabolic adaptation.

960